Engineering Structures 333 (2025) 120130

Contents lists available at ScienceDirect

Engineering Structures

journal homepage: www.elsevier.com/locate/engstruct

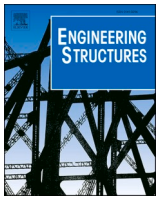

A novel cable-pulley based self-centering energy dissipation (CP-SCED) brace for seismic induced damage mitigation of RC double-column bridge piers

Huailei Qin [a], Gabriele Milani [b,1], Kaiming Bi [c,d,*,1], Huihui Dong [a], Xiuli Du [a]

[a] State Key Laboratory of Bridge Safety and Resilience, Beijing University of Technology, Beijing 100124, China
[b] Department of Architecture, Built Environment and Construction Engineering (ABC), Politecnico di Milano, Piazza Leonardo da Vinci 32, Milan 20133, Italy
[c] Department of Civil and Environmental Engineering, The Hong Kong Polytechnic University, Kowloon, Hong Kong, China
[d] Research Centre for Urban Hazards Mitigation (RCUHM), The Hong Kong Polytechnic University, Kowloon, Hong Kong, China

ARTICLE INFO

Keywords:
CP-SCED
Hysteretic characteristics
RC double-column bridge piers
Partial self-centering

ABSTRACT

An innovative cable-pulley based self-centering energy dissipation (CP-SCED) brace with adjustable hysteresis parameters is proposed in the present study. It is designed to control seismic induced damages to engineering structures, with the aim of balancing different damage indicators for the structure. The proposed CP-SCED brace consists of a self-centering system, an external friction energy dissipation system and a cable-pulley system. The corresponding purposes are to provide self-restoring force, dissipating energy, and adjusting post-yield stiffness, respectively. The overall configuration, working mechanism and restoring-force model of this brace are first introduced. A simplified specimen is designed, manufactured and tested to validate the analytical model. Parametric studies are conducted to explore the influences of the key brace parameters on the hysteretic performance. Subsequently, the brace is applied to an RC double-column bridge pier, and system-level parametric analyses are carried out to evaluate the roles of different brace design parameters. Based on which, optimal parameters are recommended and verified. Finally, a 'partial self-centering' CP-SCED brace, which allows for certain static residual deformation, is identified as suitable for achieving a reasonable balance between the peak and residual deformations of the structure. Compared to the bare pier, the average peak and residual drift ratios are reduced by 66.14 % and 91.55 %, respectively. Moreover, the average base shear force of bridge piers with the brace recommended in this study is 93.22 % of that of piers with traditional SCED braces.

1. Introduction

Residual deformation is an important indicator for evaluating the functionality of a civil engineering structure after a severe earthquake. As indicated by some researchers (e.g., McCormick et al. [1]), if the post-earthquake residual drift ratio of a structure exceeds 0.5 %, reconstruction becomes more economical than repair. Moreover, a residual drift ratio beyond 1.0 % will significantly elevate the risk of structural collapse during aftershocks [2]. Yousef-beik et al. [3] pointed out that the residual displacement could be a critical seismic design parameter when the economic losses such as the cost for realignment and repair is taken into account. Therefore, enhancing the seismic performance of a structure requires reducing the maximum seismic response to limit the extent of damage. It also involves minimizing the residual deformation to improve the economic feasibility for repairs.

Self-centering energy dissipation (SCED) braces have been demonstrated effective in controlling both the peak and residual displacements of engineering structures [4]. Generally, these SCED braces consist of two main parts: the self-centering (SC) system and the energy dissipation (ED) system. In particular, the SC system aims to restore the structure to its original position, while the ED system mitigates peak displacement by dissipating seismic energy. Common SC systems include disc springs [5,6], shape memory alloys (SMAs) [7–9], high-strength prestressed tendons [10,11], etc. It is noteworthy that within the SC system, a limited amount of energy is often dissipated due to friction between different components. However, this amount of energy is typically

* Corresponding author at: Department of Civil and Environmental Engineering, The Hong Kong Polytechnic University, Kowloon, Hong Kong, China.
E-mail address: kaiming.bi@polyu.edu.hk (K. Bi).

[1] The second and third authors are editors of this journal, In accordance with policy, Gabriele Milani and Kaiming Bi were blinded to the entire peer review process.

https://doi.org/10.1016/j.engstruct.2025.120130
Received 25 June 2024; Received in revised form 16 February 2025; Accepted 11 March 2025
Available online 29 March 2025

unstable and uncontrollable. For the ED system, metals (through yielding) [12,13], friction-based devices [14,15], and viscoelastic materials [16–18] have been widely used. The hysteresis curves of such ED elements typically exhibit full rectangular or elliptical shapes, indicating excellent ED capability. It is worth noting that, compared to braces that dissipate energy through metals and friction, the viscoelastic materials result in lower non-structural damage to the structure [19]. A SCED brace can be formed by connecting a SC system and an ED system in parallel. The force-displacement curve of a SCED brace is normally characterized by four crucial parameters as shown in Fig. 1, namely, the initial stiffness (K_1), yield strength (F_y), post-yield stiffness (K_2), and energy dissipation ratio (β). The initial stiffness K_1 is inherently tied to the elastic modulus of the brace elements, such as the inner and outer tubes, and thus cannot be easily adjusted [20]. The post-yield stiffness K_2 corresponds to the stiffness of the self-centering material and is generally fixed once the material is determined. As for the yield strength F_y, it is influenced by both the pre-compressive force of the SC system and the initial activation force of the ED system. It is generally found that maintaining β unchanged, increasing F_y requires raised pre-compressive force of the SC system and thus reduces its ultimate deformation, which is not advised normally. On the other hand, when F_y is fixed, changing β (which varies from 0.0 to 2.0 [21]) significantly affects the energy dissipation capacity and self-restoring force (F_r) of the brace. Under extreme circumstance β equals to 0.0, indicating an elastic bilinear system with no energy dissipation (Fig. 1(a)). In this case, $F_r = F_y$. On the other hand, $\beta = 2.0$ means an idealized elastoplastic behavior with full hysteresis (Fig. 1(e)), resembling the commonly used buckling restrained braces (BRBs) [22,23], exhibiting maximum energy dissipation capacity but null self-centering ability. This design may even increase the structural residual deformation as indicated in some studies (e.g., [24]). For the case where $0 < \beta \leq 1.0$, as shown in Fig. 1(b), a typical flag-shaped hysteresis curve is observed, with no residual deformation being obtained. It is worth note that, upon installation to a structure, the brace provides large self-restoring force but with constrained energy dissipation capacity. When β is precisely 1.0 (Fig. 1(c)), the self-centering system provides just enough restoring force within the brace to ensure zero residual deformation. However, under static conditions, the brace cannot contribute a restoring force to the structure to reduce its residual displacement. When β falls within the range of 1.0 and 2.0 (Fig. 1(d)), a 'pinching-like' behavior is observed in the hysteretic loop, resulting in certain residual deformation after static unloading, despite the self-centering element continues to provide self-restoring force. This behavior is also dubbed 'partial self-centering'.

The applications of SCED braces have been extensively investigated due to their outstanding seismic performances and the capability for quick replacement after a severe earthquake. The researches primarily focused on buildings [4,25–29]. In recent years, there has been a growing interest in applying them on bridge structures [20,30–34]. For example, Dong et al. [20] emphasized the significant influences of K_1, F_y, K_2 and β on the seismic performance of bridge structures. It was found that a brace with large K_1, F_y, and K_2 generally reduces both the peak and residual drift ratios of the bridge but may increase the shear force in the columns due to the increased acceleration. Additionally, a large β normally minimizes the peak displacement response but may result in large residual deformation owing to the insufficient self-restoring force. Its influence on the column shear force was found minor. In summary, brace parameters significantly influence structural responses, and it is crucial to consider different damage indicators simultaneously during the brace design. However, in [20], when the influence of one parameter was examined, the other parameters were assumed unchanged to preclude the combined effect. In reality, the hysteretic parameters of SCED braces are not independent, and the combined effect of brace parameters on the structure should be thoroughly studied. For instance, a higher post-yield stiffness enhances collapse capacity and reduce the peak and residual displacement response, but it will increase shear force demand. Regarding the energy dissipation ratio, maintaining a constant F_y, a larger β may increase the structural residual deformation. However, it also dissipates more seismic energy, consequently reducing the peak displacement [35–37]. Therefore, adjusting design parameters to achieve a good balance between different damage indicators is important to minimize seismic induced damage to structures.

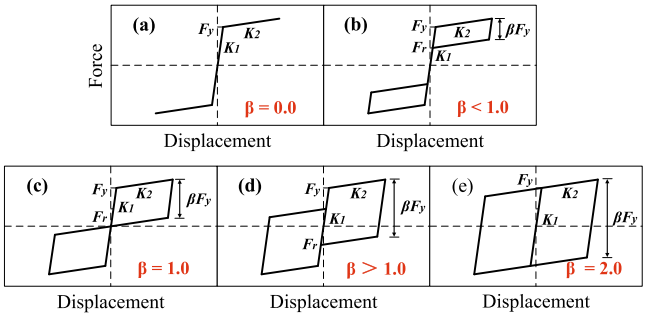

Fig. 1. Possible force-displacement curves of a SCED brace.

Though the hysteretic behavior of an SCED brace significantly influences the structural responses, the brace parameters in most previous studies were fixed and un-adjustable. Some scholars [15,21,38] proposed braces capable of adjusting the extent of energy dissipation, the post-yield stiffness K_2, however, remains fixed. This inherent inflexibility hampers their applications in engineering practices. As mentioned earlier, during the design phase, it is essential to comprehensively consider the coupling effects between the brace design parameters and different damage indicators. This approach helps balance safety and performance, ultimately achieving the optimal earthquake resistant design. Therefore, this paper introduces a cable-pulley based self-centering energy dissipation (CP-SCED) brace with adjustable parameters (including F_y, K_2 and β), enabling flexible adjusting the brace hysteresis performance based on varying requirements.

This study introduces the CP-SCED brace, which innovatively incorporates the cable-pulley system to adjust the brace post-yield stiffness. The reliability of the cable-pulley systems has been well-documented in previous research. For instance, Hernandez et al. [39] used an energy dissipation device consisting of a cable-pulley system in series with a spring-damper device (fluid viscous type) to achieve high damping ratios across all structural modes of buildings. Shake table and pullback tests on a scaled five-story building demonstrated the system performance, validating the feasibility of this design. Jung et al. [40] proposed a displacement amplification damping system aimed at maximizing damper performance. This system consisted of steel wire ropes, pulleys, and a viscous damper. Experimental results showed that the pulley system could significantly amplify the damper displacement. Majima et al. [41] introduced the Movable Pulley Damper System (MPDS), a passive vibration control system that utilizes a block-and-tackle amplification mechanism. By amplifying wire movement, this system enhances energy dissipation in the damper. Shake table tests conducted on a scaled building model revealed that the MPDS significantly reduced seismic response while effectively amplifying damping effects. Additionally, Majima et al. [42] further developed the Pulley Damper Ceiling System (PDCS), which combined two pulley tackle mechanisms, a passive energy dissipation device, and a suspended ceiling system (SCS). Full-scale shake table tests demonstrated that the PDCS amplified damper displacements and velocities, considerably reducing displacement and acceleration responses compared to conventional and braced SCSs.

Because of the diverse hysteresis performance of braces and their significant impact on structural responses, rational design of brace parameters has become a key focus of research. Dong et al. [33], utilizing the concept of 'structural fuse', argued that when the self-restoring force

F_r of the brace is greater than or equal to the yield force of the structure, the brace can pull the structure back to its original position, thus achieving (full) self-centering. Quasi-static test results demonstrated the validity of this design approach [33]. However, this design method was proposed based on the static equilibrium. Under dynamic excitation, this design tends to be conservative. This is because the actual residual deformation of an engineering system during dynamic shakedown is smaller than the maximum possible residual deformation obtained by slowly removing the load with the same peak displacement [43]. As a result, the static design method underestimates the self-centering ability of braced structures. In fact, Wang et al. [21] pointed out that due to the existence of 'probabilistic self-centering,' a structure tends to return to its original position; Fang et al. [44] and Atasever et al. [45] further indicated that a 'partial self-resetting' device can keep a good balance between the structural and non-structural damages of buildings, offering a more promising solution. Very recently, the authors [46] conducted shake table tests on RC double-column bridge piers with and without SCED brace. The brace was designed according to the static method. The tests results demonstrated that the brace significantly reduced the peak displacement response of the pier and effectively controlled the residual deformation. However, it was also observed that the brace did not fulfill its complete energy dissipation role. Hence, it is worth exploring whether it is necessary to design braces based on the concept of 'complete self-centering'.

To address the above challenges, an innovative CP-SCED brace with adjustable hysteresis parameters is proposed in this paper. The configuration, working mechanism and restoring-force model of such a brace are first described. Subsequently, a simplified specimen is designed, manufactured and tested to verify the analytical model of the brace. Component-level parametric analyses are then performed to illustrate the variable hysteretic behavior of the brace. Finally, system-level analyses are conducted on braced piers, considering the coupling effects of brace parameters and different damage indicators. Optimal brace parameters are recommended to enhance both structural resilience and damage mitigation, ensuring the safety and performance of the bridge pier during seismic events.

2. CP-SCED brace

2.1. Brace configuration

Fig. 2 presents the configuration and exploded views of the proposed CP-SCED brace. It can be seen that this brace comprises of a self-centering system, an external friction energy dissipation system and a cable-pulley system. These systems are used to provide self-restoring force, dissipate energy, and adjust post-yield stiffness, respectively. Each system is discussed in detail in this section.

The self-centering system, as shown in Fig. 2(b), mainly includes two groups of disc springs, an internal shaft, an external tube, and other necessary accessories such as the shim plates, ear plates, and end plates. The upper end of the external tube and the lower end of the internal shaft are individually welded to the corresponding end plates, leaving the opposite ends free. The self-restoring force is achieved by applying pre-compressive force to the disc springs.

Fig. 2(c) illustrates the configuration of the cable-pulley system. Note that, for simplicity, this figure depicts the most basic arrangement of the cable-pulley system. The fixed pulleys are mounted on shim plate 1 and the middle shim plate, respectively. The cables pass through the reserved holes in shim plates 1, 2 and 4, with their two ends fixed to another shim plate 1. The middle shim plate, welded to the external tube, can track the movement of the external tube. In the center of the middle shim plate, an aperture is provided to allow it to pass through and smoothly slide along the internal shaft. Shim plates 4 are designed to prevent cable misalignment. Whether the brace is either tensioned or compressed, only the deformation of the disc spring group on one side is amplified by a factor of two, leading to a 1.5-fold increase in the post-

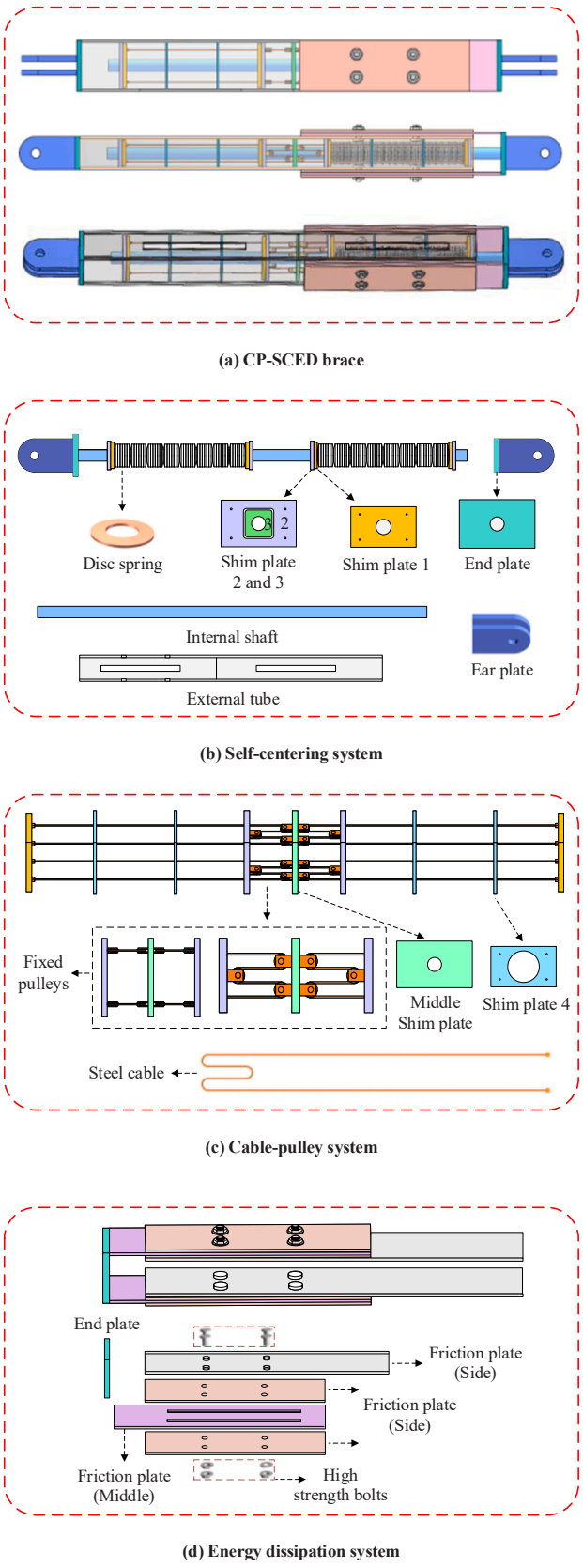

Fig. 2. (a) Overall view of the proposed CP-SCED brace; (b) self-centering system; (c) cable-pulley systems and (d) energy dissipation system.

yield stiffness of the brace. The detailed relationship between the amplification factor and the pulley arrangement will be discussed in Section 3.2.

In this brace, energy dissipation primarily relies on the external friction energy dissipation devices (Fig. 2(d)), spatially separated from the disc spring zone. This separation allows for easy inspection and replacement if necessary. As depicted above, the middle friction plates are directly fixed to the end plate, while the side friction plates are secured to the external tube using high-strength bolts. When the internal shaft and external tube experience relative movement, the middle and side friction plates slide against each other, leading to energy dissipation through friction. The amount of dissipated energy depends on both the friction coefficient and the preload applied to the high-strength bolts.

It is evident that in practices, friction between the compacted disc springs, and between the disc springs and the internal shaft, is inevitable. Consequently, the self-centering system also dissipates some energy. In other words, even when the pre-tightening force of the bolt in the energy dissipation device is zero, the hysteresis curve of the brace will still exhibit a flag shape. The subsequent experiments confirmed this observation.

2.2. Working mechanism

Fig. 3(a) illustrates the working mechanism of the CP-SCED brace. Assuming the left end of the brace is fixed (see the orientation in the figure), when the right end plate is under compression, the left side of the disc spring groups are held in place by shim plate 2, which is welded on the external tube. Simultaneously, shim plate 3, welded on the internal shaft, compresses the disc spring groups, resulting in the brace being compressed. Upon unloading, the disc springs are capable of bringing the deformed brace back to its original position, thus achieving self-centering capability. During this process, the energy dissipation system works in parallel with the self-centering system. The middle friction plates of the external friction device slide leftward along with the right end plate, while the side friction plates remain fixed to the external tube, and these friction plates experience relative sliding and dissipate energy. Conversely, when the right end plate is under tension, the working principle is the same but in the opposite direction as under compression. For conciseness, the details are not repeated.

For the cable-pulley system, when the middle shim plate moves to the left, it drives the pulleys fixed on it to move. Conversely, the pulleys fixed on the shim plate 1 remain stationary. Tension force develops in the cable, thus amplifies the displacement of the opposite side of shim plate 1. This amplified displacement results in an increased deformation of the disc spring groups, enhancing the bearing capacity without altering the overall brace displacement. Consequently, the stiffness of the brace is increased. It is crucial to note that during tension or compression of the brace, only one side of the cable-pulley system participates in the amplification process, as will be detailed in the subsequent subsection. It is worth noted that adjusting the number of fixed pulleys allows for the attainment of different disc spring deformation amplification factors. Fig. 3(b) presents schematic diagrams for other arrangement forms, with the deformation of the disc spring group being amplified by a factor of two to four, respectively.

Additionally, it should be emphasized that the post-yield stiffness of the brace can also be altered by changing the configuration of the disc springs, such as varying the number of disc springs stacked in parallel or in series. However, this would complicate the stacking of the disc springs. Moreover, for the proposed brace, the two disc spring groups are welded and fixed within the brace, making it impossible to adjust the post-yield stiffness by modifying the disc spring groups after assembly. Since this study focuses on developing a brace with adjustable hysteretic parameters, the role of the cable-pulley system in adjusting the post-yield stiffness is crucial.

For the CP-SCED brace, disc springs are used to provide the restoring force, friction between the friction plates is used to provide energy dissipation capability, and cable-pulley is used to adjust the post-yield stiffness. In practice, the limitations of disc springs and friction in the traditional systems also exist in this system. For example, the deformation capability of disc springs is normally limited: according to the Chinese Standard [47], the deformation of a single disc spring should not exceed 75 % of its maximum allowable deformation; Wear may appear between the friction plates when relative movements occur. The major difference of the present design and traditional systems lies in the cable-pulley system. As shown in Fig. 2, the structure of the cable-pulley is actually quite simple, and its function is solely to amplify the deformation of the individual disc spring group, thereby increasing the post-yield stiffness of the brace. The limitation of this system might lie in the internal space of the brace, which must be able to accommodate the fixed pulleys and the cables.

3. Analytical model

Based on the configuration and work principle of the CP-SCED brace, its force-displacement relationship can be conveniently predicted by considering the changes in the stiffness of the bracing system at different stages. This section formulates the hysteretic curve.

3.1. Initial stiffness and activation deformation

For the CP-SCED brace, its initial stiffness, denoted as K_1, is controlled by the stiffness of the internal shaft (K_{int}) and external tube (K_{ext}). Therefore, the values of K_1 and the bearing force P at a given deformation of δ (the brace is not activated at this time) can be expressed as follows:

$$K_1 = \frac{k_{int}\, k_{ext}}{k_{int} + k_{ext}} \tag{1}$$

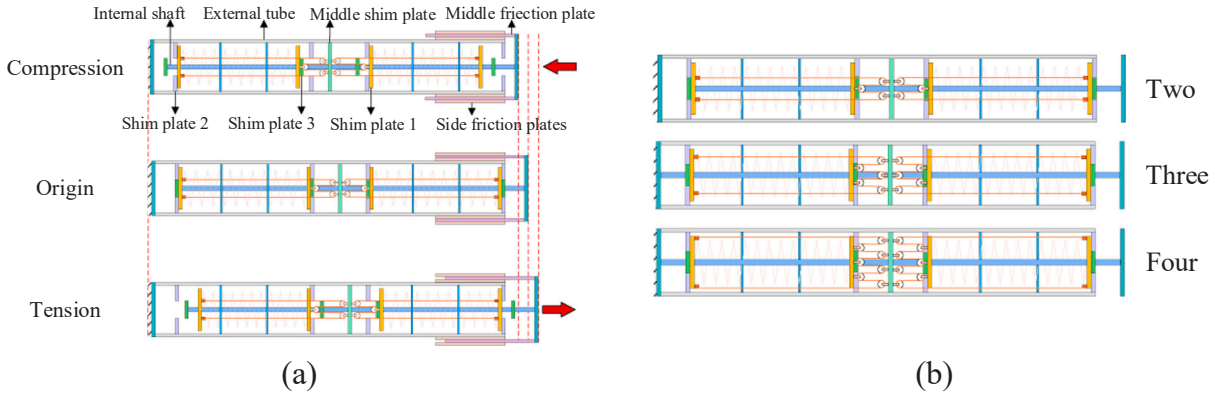

Fig. 3. (a) Working mechanism of the brace, and (b) Different configurations of the cable-pulley systems.

$$P = \delta K_1 \tag{2}$$

and the activation deformation, δ_0, is given by

$$\delta_0 = \frac{F_y}{K_1} = \frac{P_0 + F_0}{K_1} \tag{3}$$

where F_y is the yield force of the brace, P_0 is the initial pre-compressive force for the two disc spring groups (the self-centering system), and F_0 is the force required to activate the two external friction devices.

3.2. Post yield stiffness

Fig. 4 illustrates the relationship of using the cable-pulley system to amplify the disc spring group deformation. For clarity, this diagram gives the simplest arrangement of the cable-pulley system. As mentioned before, no matter the brace is under tension or compression, only the cable-pulley system on one side works. Therefore, only the schematic diagram of the left half of the cable-pulley system is given here.

As shown, assuming the length of a single cable between the shim plate 2 and the middle shim plate is δ_1, and that between the two shim plates 1 is δ_2, the total length of the cable is thus $4\delta_1 + 2\delta_2$. When the middle shim plate moves δ_Δ to the right, the length of a single cable between the shim plate 2 and middle shim plate becomes $\delta_1 + \delta_\Delta$, and the length of a single cable between the two shim plates 1 becomes:

$$\frac{(4\delta_1 + 2\delta_2) - 4(\delta_1 + \delta_\Delta)}{2} = \delta_2 - 2\delta_\Delta \tag{4}$$

To quantitatively show the amplification relationship, assuming $\delta_2 = 4\delta_1$, $\delta_\Delta = \delta_1$, $\delta_2 - 2\delta_\Delta$ in Eq. (4) is then $2\delta_1$. In other words, when the middle shim plate moves δ_1 to the right, the disc spring group is compressed by $2\delta_1$. Previous experiments [38] have shown that the hysteretic behavior of the disc spring group can be approximately considered as linear elastic. Thus, the bearing capacity of the disc spring group is magnified by a factor of 2 from its original bearing capacity (F_1) with no deformation amplification. As a result, the bearing capacity of the brace, which consists of two disc spring groups connected in parallel, becomes $3F_1$ ($F_1 + 2F_1 = 3F_1$). In contrast, the brace without the cable-pulley systems has a bearing capacity of $2F_1$ ($F_1 + F_1 = 2F_1$) under the same deformation. Therefore, the post-yield stiffness of the brace with cable-pulley systems is magnified 1.5 times ($3F_1/2F_1 = 1.5$). By further increasing the number of fixed pulleys, different stiffness amplification factors can be achieved. In general, if the number of the pulleys fixed on the middle shim plate (the displacement amplification factor) is n, the post-stiffness of the brace then will be amplified by $(n+1)/2$ times.

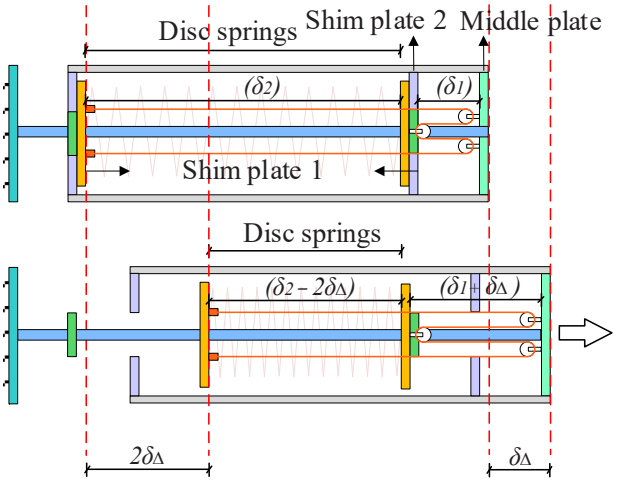

Fig. 4. Working principle of the cable-pulley system for amplifying the disc spring group deformation.

With one end of the brace fixed, applying a deformation δ ($>\delta_0$) to the opposite end results in relative movement between the inner core and the outer tube. This causes the stiffness of the brace changing from the initial stiffness K_1 to the post-yield stiffness K_2, which is determined by the disc spring groups and the cable-pulley systems as discussed above. At this time, the brace bearing force P is provided by the external friction energy dissipation devices and the disc spring groups. In other words, P is the sum of the initial pre-compressive force for the self-centering system P_0, the force required to activate the two external friction devices F_0, the bearing capacity of the disc spring group without deformation amplification P_{d1}, and the bearing capacity of the disc spring group with deformation amplification P_{d2}. Namely, P can be expressed as follows:

$$P = P_0 + F_0 + P_{d1} + P_{d2} \tag{5}$$

The bearing capacity P_d of any disc spring group can be calculated according to the Chinese code [47] by using the following formula:

$$P_d = \frac{p}{1 - f_M(p-1) - f_f} \frac{4E}{1-\mu^2} \frac{t^4}{M_1 D^2} M_4^2 \frac{f}{t}\left[M_4^2\left(\frac{h_0}{t} - \frac{f}{t}\right)\left(\frac{h_0}{t} - \frac{f}{2t}\right) + 1\right] \tag{6}$$

As discussed above, during the operation of the brace, the deformation of only one disc spring group is amplified n times. Consequently, P_{d1} and P_{d2} are:

$$P_{d1} = P_d \tag{7}$$

$$P_{d2} = nP_d \tag{8}$$

As shown, quite a few parameters exist in Eq. (6). The detailed information for these parameters can be found in code [47]. For completeness, they are briefly introduced herein:

In Eq. (6), f is the deformation of one piece of disc spring. It is related to the brace deformation δ, the brace activation deformation δ_0, and the initial pre-compressive deformation of the disc spring groups δ':

$$f = \frac{\delta - \delta_0 + \delta'}{i} \tag{9}$$

where p (in Eq. (6)) and i (in Eq. (9)) represent the numbers of disc springs stacked in parallel and in series, respectively.

The parameters f_M and f_f in Eq. (6) are the friction coefficients of the disc spring cone and bearing edge, respectively. E denotes the Young's modulus of the disc springs, and μ is the Poisson's ratio. D is the outer diameter of the disc-spring. t and h_0 are the thickness and solid height of one section of the disc springs without a bearing surface. It should be noted that, when disc springs with the bearing surface are installed in the brace, t and h_0 in Eq. (6) should be replaced by t' and h_0', which are the thickness and solid height of one piece of the disc springs with a bearing surface, respectively [47].

In addition, the coefficient M_1 in Eq. (6) can be calculated by Eq. (10). For M_4, it is equal to 1.0 for a disc spring without bearing surface, while for the disc spring with a bearing surface it can be calculated based on Eqs. (11)-(13).

$$M_1 = \frac{1}{\pi} \frac{[(C-1)/C]^2}{(C+1)/(C-1) - 2/\ln C}, \quad C = \frac{D}{d} \tag{10}$$

$$M_4 = \sqrt{-\frac{C_1}{2} + \sqrt{\left(\frac{C_1}{2}\right)^2 + C_2}} \tag{11}$$

$$C_1 = \frac{(t'/t)^2}{[(1/4)(H_0/t) - t'/t + 3/4][(5/8)(H_0/t) - t'/t + 3/8]} \tag{12}$$

$$C_2 = \frac{C_1}{(t'/t)^3}\left[\frac{5}{32}\left(\frac{H_0}{t}-1\right)^2+1\right] \tag{13}$$

Thus, the post-yield stiffness K_2 of the brace can be expressed as:

$$K_2 = 2K_{ds}\frac{n+1}{2} = 2\frac{p}{1-f_M(p-1)-f_f}k_s\frac{n+1}{2}$$
$$= (n+1)\frac{p}{1-f_M(p-1)-f_f}\frac{4E}{1-\mu^2}\frac{t^3}{M_1D^2}M_4^2\left\{M_4^2\left[\left(\frac{h_0}{t}\right)^2-3\frac{h_0 f}{t\,t}+\frac{3}{2}\left(\frac{f}{t}\right)^2\right]+1\right\} \tag{14}$$

In Eq. 14, K_{ds} is the stiffness of one disc spring group; k_s is the stiffness of one piece disc spring. $p/(1-f_M(p-1)-f_f)$ represents the combination of disc springs. Additionally, there are two disc spring groups, thus the brace stiffness should be multiplied by a factor of 2.

3.3. Unloading stiffness and energy dissipation ratio

To examine the unloading stiffness and the corresponding bearing force, a typical flag-shaped hysteretic curve shown in Fig. 1 is replotted herein, and it is shown in Fig. 5, in which K_1 and K_2 represent the initial stiffness and post-yield stiffness of the brace as derived earlier. Unloading begins when the brace reaches the maximum deformation (point 'b' in the figure), and the direction of friction reverses at this moment, resulting in the brace proceeding from point 'b' to point 'c'. Namely, the energy dissipation section (b-c) appears. This phase bears similarity to the brace in the initial state, the stiffness during this interval is thus approximately equal to K_1 [38]. The magnitude of this energy dissipation segment is denoted as βF_y. On the other hand, a force of $2F_0$ must be overcome during this process to facilitate the sliding of the internal shift and external tube pasting each other once more. Namely, the extreme condition $\beta F_y = 2F_0$ should be satisfied, β thus can be calculated as:

$$\beta = \frac{2F_0}{F_y} = \frac{2F_0}{P_0+F_0} \tag{15}$$

where, F_b and F_c are the forces at point 'b' and point 'c', respectively.

When the friction system is activated again, the stiffness of the brace is governed by the disc spring groups and cable-pulley systems, which can be considered approximately equal to K_2. As the unloading deformation reaches the point of self-restoring force 'd', it proceeds to return to the original point 'o' along the initial stiffness K_1. Similarly, the behavior of the CP-SCED brace under compression is the same as its in tension and will not be discussed further. It should be noted that the hysteretic behavior of the brace calculated based on theoretical model is symmetric. If a real hysteretic curve exhibits non-symmetric behavior, the theoretical model should be re-derived based on the realistic hysteretic behaviors of the brace.

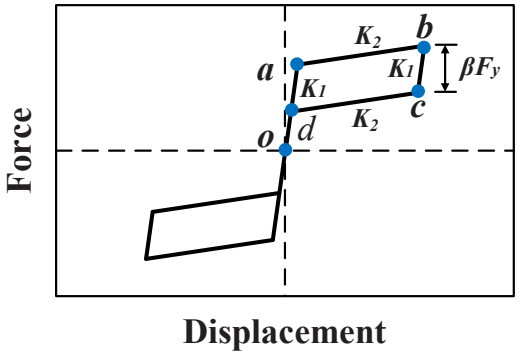

Fig. 5. Typical hysteresis curve of a CP-SCED brace.

4. Model validation and parametric analysis

4.1. Model validation

The authors recently completed a quasi-static test on a SCED brace. The test specimen represents a special case of the CP-SCED brace as proposed in the present study. In particular, this specimen did not include the energy dissipation device and cable-pulley system; it solely featured by a self-centering system, as shown in Fig. 2(b). The specimen was designed with a yield force of 47 kN and a maximum deformation of 40 mm. It includes a total of 240 disc springs, divided into two parallel groups. This specimen could provide a self-restoring force of 39 kN. For convenience, we use this experiment to verify the accuracy of the proposed model. Further details about the test can be found in the authors' recent article [46].

Fig. 6(a) shows the test setup. As shown, the quasi-static displacement was applied to the brace by a hydraulic actuator, and the corresponding force was measured by a load cell that was attached to one end of the brace. Fig. 6(b) gives the incremental amplitude loading protocol used in the tests. Displacements of 0.05, 0.125, 0.25, 0.375, 0.5, 0.75 and 1.0 times Δl (40 mm) were applied (where Δl represents the design axial deformation of the brace), and each amplitude was repeated twice.

The black line in Fig. 7 shows the hysteresis curve of the specimen obtained in the test. It is evident that the brace presents a flag-shaped hysteresis curve with excellent self-centering ability, displaying nearly no residual displacement. Some energy was dissipated during the tests, as shown, which was caused by the friction between different components of the brace.

Next, the theoretical model proposed in the previous section will be validated based on the experimental results. As the test specimen lacked cable-pulley systems, n is set to 1 (the cable-pulley system does not amplify the deformation of the disc-spring group). The other parameters for the analytical model calculation can be obtained from the experimental study [46], and they are detailed in Table 1.

The design yield strength F_y of the test specimen is 47 kN. By substituting all the above parameters into Eqs. (1)-(14), K_1, δ_0 and K_2 can be calculated to determine points 'a' and 'b' in Fig. 7. It should be noted that, the energy dissipated by the tested brace was due to the friction between different disc springs and various brace components, which cannot be straightforwardly determined as discussed above. On the other hand, in our analytical derivation as discussed in Section 3, the energy dissipated by this part is actually ignored, and the energy is assumed to be dissipated by the ED component. Even though the energy is dissipated by different components in the test and in the analytical derivation, the final effect is actually the same, and they lead to the same hysteretic curve. To quantify the energy dissipation of this part, based on the experimental data, the energy dissipation ratio of the self-centering system ($\beta_{sy-test}$) as measured in the test can be calculated using the following formula:

$$\beta_{sy-test} = \frac{F_{b-test}-F_{c-test}}{F_{y-test}} = \frac{107.16\text{kN}-95.11\text{kN}}{47\text{kN}} = 0.25 \tag{16}$$

In particular, based on the previously obtained values of K_1, δ_0 and K_2, the peak force of the theoretical model is calculated as $F_{b-model} = 104.88$kN (point 'b' in the red line of Fig. 7). Moreover, in the theoretical model, the energy dissipation ratio of the self-centering system ($\beta_{sy-model}$) is determined according to experimental results, thus $\beta_{sy-model} = \beta_{sy-test} = 0.25$. Therefore, the point 'c' in the red line of Fig. 7 can be calculated as:

$$F_{c-model} = F_{b-model} - \beta_{sy-model}F_y = 104.88\text{kN} - 0.25 \times 47\text{kN} = 93.13\text{kN} \tag{17}$$

As mentioned previously, the stiffness of segment 'bc' equals that of segment 'oa', allowing for the determination of the coordinates of point 'c'. Finally, the stiffness of phase 'cd' matches that of 'ab', enabling the

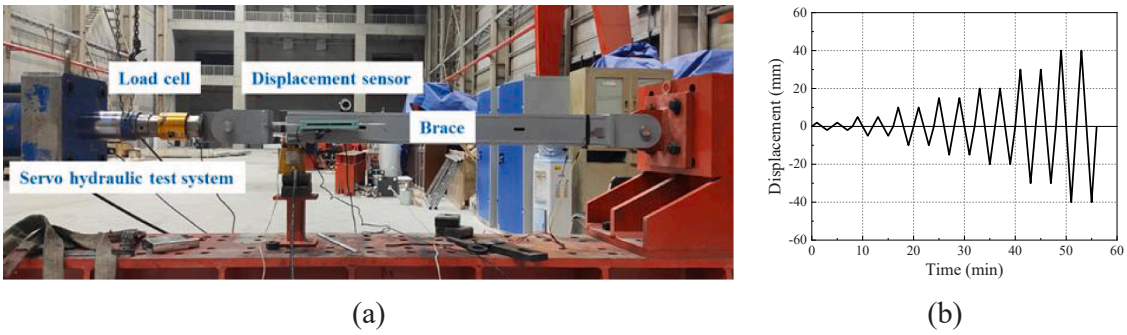

Fig. 6. Brace test: (a) test setup; (b) loading protocol.

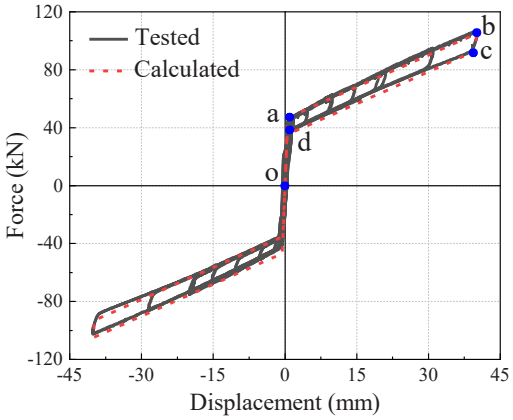

Fig. 7. Tested and calculated hysteretic curves of the brace.

determination of the coordinates of point 'd'. When the brace deformation is negative, the calculation method remains consistent with that of the first quadrant, and will not be reiterated here. With these steps completed, the hysteresis curve can be obtained, and it is depicted by the red dashed line in Fig. 7. As shown, the theoretical result matches well with the test data, especially when the applied displacement is positive (the braces is under tension). Slight difference exists when large negative displacement (under compression) is applied to the brace. This is because the testing data is not perfect and it is not symmetrical as shown in Fig. 7, while the analytical results are symmetrical. These results validate the analytical model derived above. It should be known that the hysteresis curve in Fig. 7 represents the fundamental mechanical behavior of the CP-SCED brace. By adjusting the parameters of P_0, F_0 and n, hysteretic curves with different yield strength, energy dissipation ratio and post-yield stiffness can be obtained. The following sections will investigate the effects of these parameters on the hysteresis curve.

4.2. Parametric studies

The brace hysteresis performance is influenced by various parameters of the brace. These include the initial pre-compressive force of the two disc-spring groups (P_0), the number of the pulleys fixed on the middle shim plate (n), the force required to activate the two external friction devices (F_0), disc spring friction coefficients (f_M and f_f), disc spring dimensions (D, d, t, H_0 and h_0) and their combination forms (p and i). Note that the parameter analysis is conducted based on the test specimen, thus the dimensions of the disc spring, combination forms and friction coefficients have all been fixed. Furthermore, this study aims to propose a parameter-adjustable brace, allowing for flexible utilization of its hysteretic characteristics to achieve optimal seismic performance in various structures. Specifically, the yield strength can be adjusted by modifying the pre-compression force of the disc springs in the self-centering system and the pre-tightening force of the bolts in the energy dissipation system. The post-yield stiffness can be regulated by altering the arrangement of the fixed pulleys in the cable-pulley system. Additionally, different levels of energy dissipation can be achieved by applying varying pre-tightening forces to the bolts and/or using different lubricating materials between the friction plates within the system. In practical applications, the target mechanical behavior is mainly achieved by adjusting P_0, F_0 and n, and the relationships between the components and the adjustable parameters are summarized in Table 2. Following this, parametric study is focused on these three parameters, and the results are obtained based on the analytical derivations as discussed above.

Here, it should be emphasized that for the CP-SCED brace, the friction between different components inevitably dissipates some energy. However, for this brace, the energy is mainly dissipated through ED system, while the portion of energy dissipated by the self-centering system is smaller and varies less. Hence, we can assume that the energy dissipation capacity of the self-centering system remains constant. Quasi-static testing revealed that the actual $\beta_{sy-test}$ of the self-centering system is 0.25. Therefore, the energy dissipation force of the self-centering system is always equal to $\beta_{sy-model}F_y = 0.25 \times 47\text{kN} = 11.75\text{kN}$. Since the friction energy dissipation of the self-centering

Table 2
The relationships between the components and the adjustable parameters.

Adjustable parameters	Adjustable components	Relationships
Yield strength (F_y)	Initial pre-compressive force of the two disc-spring groups (P_0) and the force required to activate the two external friction devices (F_0);	$F_y = P_0 + F_0$ (3)
Post-yield stiffness (K_2)	The number of the pulleys fixed on the middle shim plate (n);	$K_2 = 2K_{ds}\frac{n+1}{2}$ (14)
Energy dissipation ratio (β)	Initial pre-compressive force of the two disc-spring groups (P_0) and the force required to activate the two external friction devices (F_0);	$\beta = \frac{2F_0}{F_y} = \frac{2F_0}{P_0 + F_0}$ (15)

Table 1
Parameters for the analytical model derivation.

D (mm)	d (mm)	t (mm)	H_0 (mm)	h_0 (mm)	μ	E (N/mm^2)	p	i	f_M	f_f
100.00	51.00	4.00	7.00	3.00	0.30	206,000	3	40	0.03	0.05

system is not considered in the theoretical model in Section 3, the β calculation formula should be:

$$\beta = \frac{2F_0 + \beta_{sy-model}F_y}{F_y} = \frac{2F_0 + \beta_{sy-model}F_y}{P_0 + F_0} \quad (18)$$

This formula considers the effect of friction in the self-centering system on the overall energy dissipation of the brace. Additionally, the energy dissipation force of the self-centering system has been determined. Thus, in the calculations of this section, Eq. 15 is replaced by Eq. 18.

Firstly, the influence of the initial pre-compressive force of the self-centering system P_0 on the brace hysteretic performance is investigated. In the analysis, F_0 is kept at 0 kN and n is assumed as 1. P_0 varies from 27 kN to 57 kN with an interval of 10 kN.As shown in Fig. 8 (a), increasing P_0 leads to the increased brace yield strength. The post-yield stiffness is slightly reduced, measuring 1588.38 kN/mm, 1533.09 kN/mm, 1479.23 kN/mm and 1427.12 kN/mm, respectively. This reduction is attributed to the increased P_0, which results in an increase in the deformation of the single disc spring (f). According to Eq. 14, this yields a smaller K_2 value. The area enclosed by the hysteresis curve, calculated from Fig. 8(a), is shown in Fig. 8(b). It can be seen that the amount of energy dissipation is nearly the same. Minor discrepancies occur due to variations in K_2, resulting in different areas of the parallelograms. However, it should be noted that, though the energy dissipation remains unchanged, β value is actually not a constant based on the definition in Eq. 15. The corresponding values are 0.44, 0.32, 0.25 and 0.21, respectively. The results in Fig. 8 also indicate that when the energy dissipation remains constant, the self-restoring force of the brace can be enhanced by increasing the pre-compressive force (P_0) of the disc-spring groups.

The influence of the number of pulleys n is investigated next. Keeping P_0 and F_0 unchanged, while n varies from 1 to 4, the corresponding hysteresis curves and dissipated energies are shown in Fig. 9. Note that as defined in Section 3.2, $n = 1$ means that the cable-pulley system does not amplify the deformation of the disc-spring group. It is apparent that increasing n obviously increases the brace post-yield stiffness K_2 while slightly decreases the dissipated energy. According to Eq. 18, with the yield strength and friction energy dissipation held constant, the β remains unchanged at its value of 0.25. It is important to note that increasing the brace post-yield stiffness will reduce the peak displacement response of the bridge pier. It, however, also raises the risk of damage to the bridge pier since the shear force will be increased. Therefore, it is important to consider the balance between the effectiveness and safety during the design phase of the brace to ensure it delivers the best overall performance.

The influence of the force required to activate the two external friction components F_0 is also assessed. Keeping P_0 (47 kN, as per the test) and n (1) unchanged, different F_0 values (0 kN, 10 kN, 20 kN and 40 kN) are considered. Fig. 10(a) presents the hysteresis curves for different F_0 values. It can be seen that as F_0 increases, F_y gradually increases while the K_2 remains unchanged. Additionally, the area enclosed by the hysteresis loop gradually increases, indicating that the brace can dissipate more energy. Fig. 10(b) shows the corresponding energy dissipation. Moreover, the β also increases gradually. The increase in yield strength and energy dissipation both contribute to reducing the peak displacement response of the structure.

It follows from Eq. 18 that keeping the yield strength F_y a constant, by simultaneously adjusting the values of P_0 and F_0, different β can be achieved. For instance, when maintaining F_y at 47 kN, adjusting P_0 to 47 kN, 29.375 kN, 17.625 and 5.875 kN, the corresponding F_0 are 0 kN, 17.625 kN, 29.375 and 41.125 kN, respectively. The resulting hysteresis curves are shown in Fig. 11(a). It is evident that as P_0 decreases (F_0 increases), the K_2 gradually increases, with respective values of 1468.65 kN/mm, 1566.81 kN/mm, 1634.89 kN/mm, and 1704.60 kN/mm. The reason for this change aligns with the earlier analysis on the impact of P_0, which will not be reiterated. The results also show that the hysteresis loops become wider when P_0 decreases, representing more energy being dissipated. Concurrently, F_r decreases, reaching negative values when F_0 exceeds 17.625 kN ($\beta = 1.0$, $P_0 = 29.375$ kN). Fig. 11(b) illustrates the change in energy dissipation, showing a gradual increase in the amount of energy dissipation. The β also increases gradually, with values of 0.25, 1.0, 1.5, and 2.0, respectively. In summary, although increasing F_0 can enhance the brace energy dissipation capacity and reduce the peak displacement response of the structure, it cannot provide sufficient self-restoring force to minimize residual deformation. Therefore, in design, the goal should be set to enhance the energy dissipation capacity of the brace while simultaneously meeting the requirements for structural residual deformation, thereby maximizing its efficiency.

The above parametric studies reveal that, by modulating parameters P_0, n and F_0, various hysteresis curves with different yield strengths, post-yield stiffness and energy dissipation capacities can be generated. Subsequently, a case study of a bridge pier will be conducted to determine optimal parameters for the brace, thereby maximizing its control effectiveness.

5. Influences of CP-SCED brace design parameters on the seismic performances of bridge piers

The authors [46] tested a double-column bridge pier very recently to investigate the performance of the SCED brace as discussed in Section 4.1. Note that due to the limitation of experimental conditions, the test model was scaled down to a ratio of 0.2. In this section, the finite element (FE) model developed in OpenSEES software (version 2.4.4) is validated using the test results. The same method is employed to establish the prototype bridge pier model, where the proposed brace is

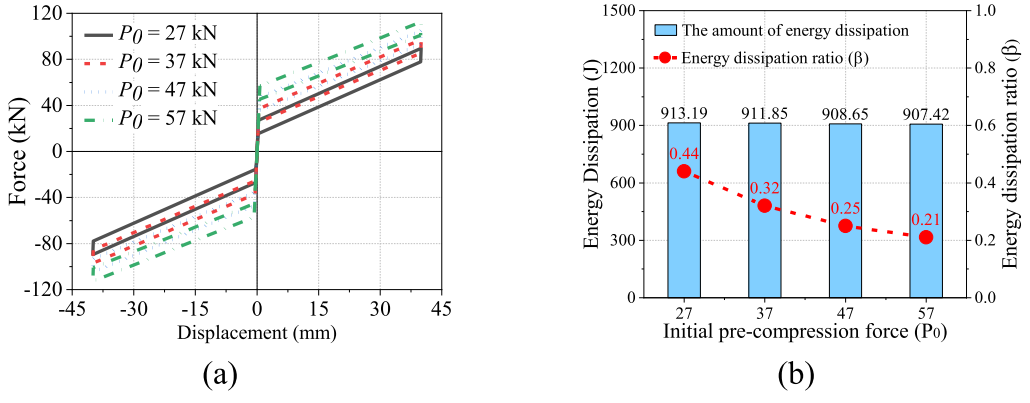

Fig. 8. Influence of P_0 on the (a) hysteretic shape and (b) energy dissipation.

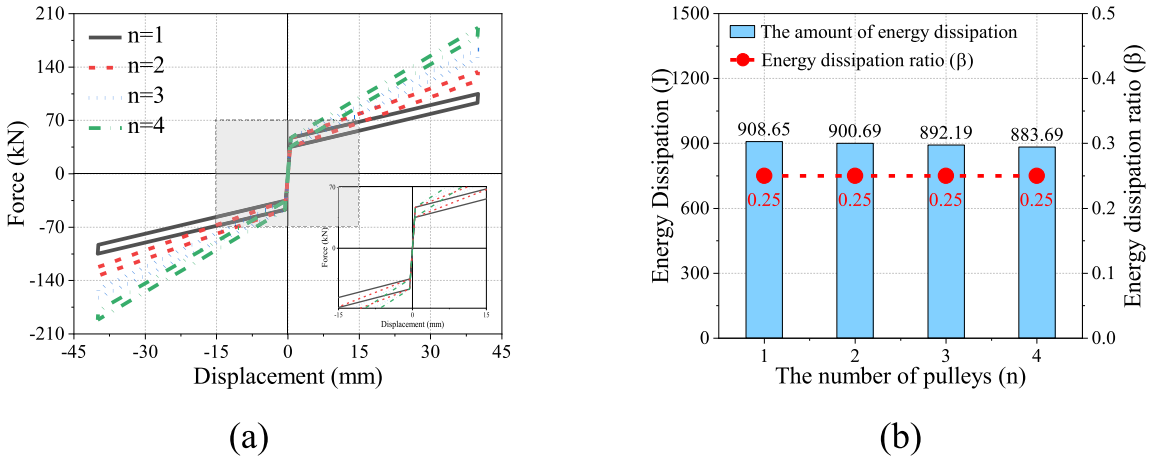

Fig. 9. Influence of n on the (a) hysteretic shape and (b) energy dissipation.

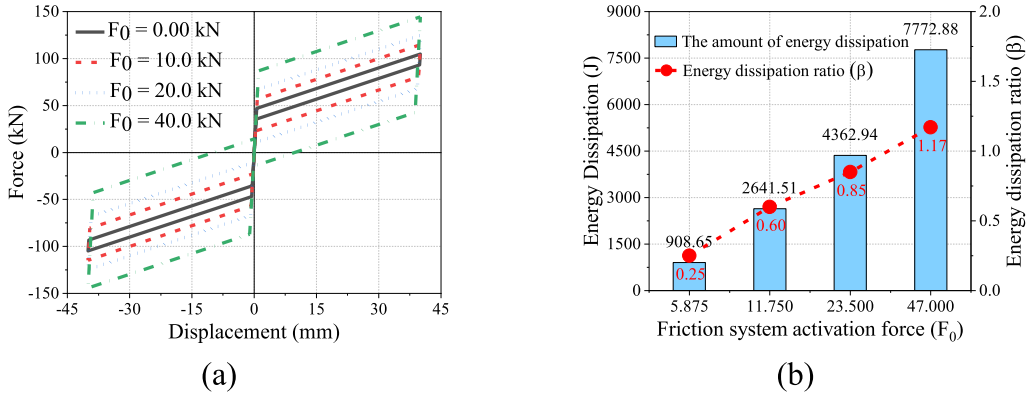

Fig. 10. Influence of F_0 on the (a) hysteretic shape and (b) energy dissipation.

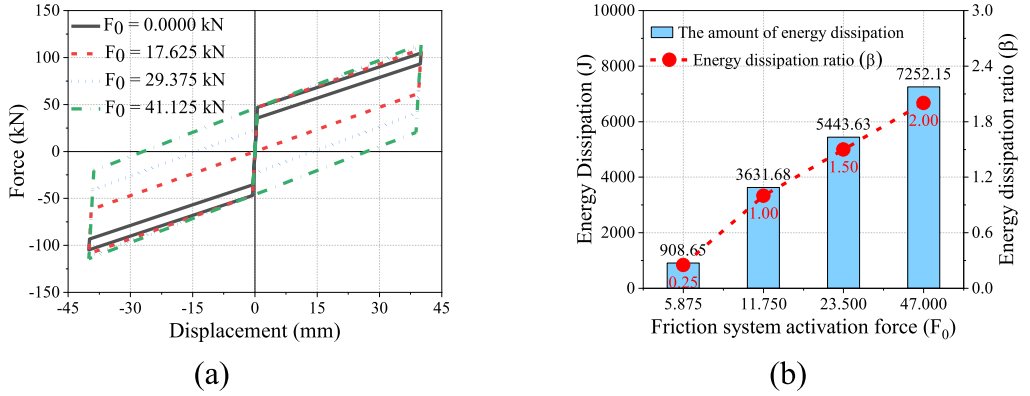

Fig. 11. Influence of F_0 on the (a) hysteretic shape and (b) energy dissipation when F_y is unchanged.

applied to the bridge pier, and the influences of the key brace parameters on the seismic responses are investigated.

5.1. Bridge pier and numerical model

Fig. 12 gives the details of the prototype bridge pier. As shown, the column has a diameter and height of 900 and 6500 mm, respectively. Sixteen longitudinal rebars with a diameter of 24 mm are arranged around the cross section of the column, thus the longitudinal reinforcement ratio is 1.138 %. Spiral hoops, with a diameter of 20 mm and a spacing of 150 mm, are embedded within the cap beam and foundation. The square cap beam size is 1200 × 1200 mm, with a length of 15,000 mm.

Fig. 13 presents the FE model of the bridge pier with braces. In this model, the columns are modeled using the nonlinear force-based beam-column elements with fiber section, while the cap beam is developed by the elastic beam-column elements due to its elastic behavior. The column segment inserted into the cap beam is assumed to be a rigid link. Concrete 02 material is applied for both the unconfined and confined concrete, and the rebars are simulated by the Steel 02 material. As for the brace, it is modeled using truss elements with uniaxial self-centering material. The concrete properties are detailed in Table 3, and the yield

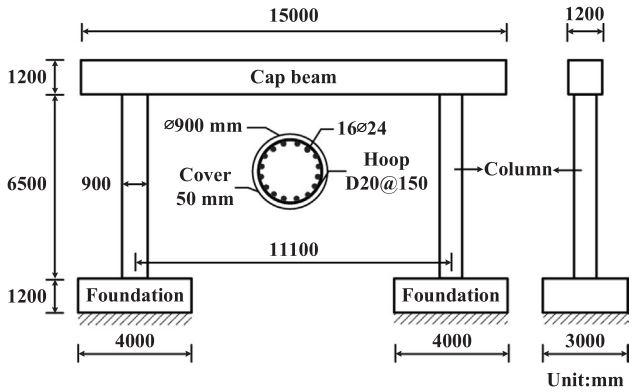

Fig. 12. Detailed dimensions of the bridge pier.

strength and ultimate strength of the longitudinal rebars are 439.76 MPa and 629.02 MPa based on experimental data. Before seismic excitation is applied, the gravity load is introduced using the "load pattern" command.

The above FE model is validated using shake table test results. It is important to note that during the tests, there was a gap between the brace and the gusset plates [46]. Consequently, when the lateral displacement of the pier was extremely small, the brace remained inactive. To replicate this scenario, a combination of self-centering material (simulating the brace) and elastic multi-linear material (replicating the gap) is employed in a series configuration. This approach is similar to strategies adopted by Qiu and Zhu [27] and Erochko et al. [48] in their brace models. Fig. 14 presents the resulting hysteresis curves, which clearly show that under small deformations, the brace force is zero. This successfully simulates the phenomenon where the brace is not activated under low excitation due to the presence of the gap. Subsequent findings have confirmed the effectiveness of this method in accurately representing real-world conditions.

The excitation for the tests was a real near-field pulse-type ground motion recorded at the Saratoga-Aloha Ave station during the 1989 Loma Prieta Earthquake. The duration of the ground motions was scaled according to similitude rules, with the PGA increased gradually from a small value (0.1 g) to a large value, under which the bare bridge pier could be severely damaged. For more information, please refer to [46]. Fig. 15 compares the lateral displacement time histories of both the bare and braced piers subjected to a typical small excitation (PGA=0.3 g) and a large excitation (PGA=0.9 g), representing the elastic and plastic damage states, respectively. The results show that under smaller excitations, the experimental and simulation data match well, but under larger seismic excitations, the results are less consistent. This discrepancy is due to the accumulated damage caused by the former smaller PGAs being considered when evaluating a larger PGA value (e.g., 0.9 g). Nonetheless, the overall agreement between the experimental and simulation results is good, confirming the precision of the developed numerical models.

Using the same modeling method, the finite element model of the prototype bridge pier (Fig. 12) is established for subsequent parameter analysis. Through the pushover analysis, the yield displacement and yield strength of the bare pier are 31.40 mm and 819.61 kN, respectively. Then, the brace for this pier is designed according to the 'full self-centering' concept. Due to space limitations, the detailed design process is not elaborated here. Interested readers can refer to the author's article [46]. The design parameters of the brace for the prototype bridge pier are listed in Table 4. It is crucial to note that the initial stiffness K_1, post-yield stiffness K_2 and energy dissipation ratio β of the full-scale brace are kept consistent with the scaled brace, following the practice documented in other literature [20]. For comparison purposes, the

Table 3
Parameters of the concrete material.

Concrete	f_c'/MPa	ε_o	f_u'/MPa	ε_u
Unconfined concrete	26.70	0.002	5.34	0.004
Confined concrete	32.02	0.0026	6.41	0.015

Note: f_c'=compressive strength; f_u'= crushing strength; ε_o=strain at maximum compressive strength; and ε_u=strain at crushing strength.

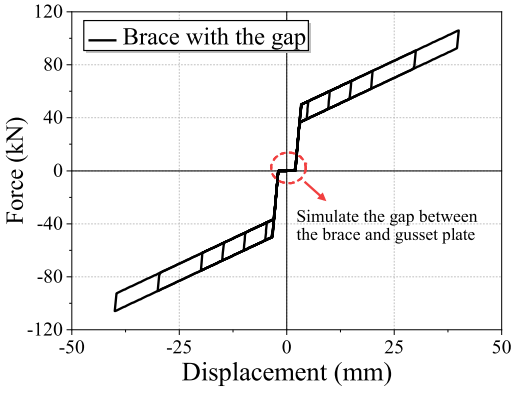

Fig. 14. Hysteresis curve of the simulated brace with the gap.

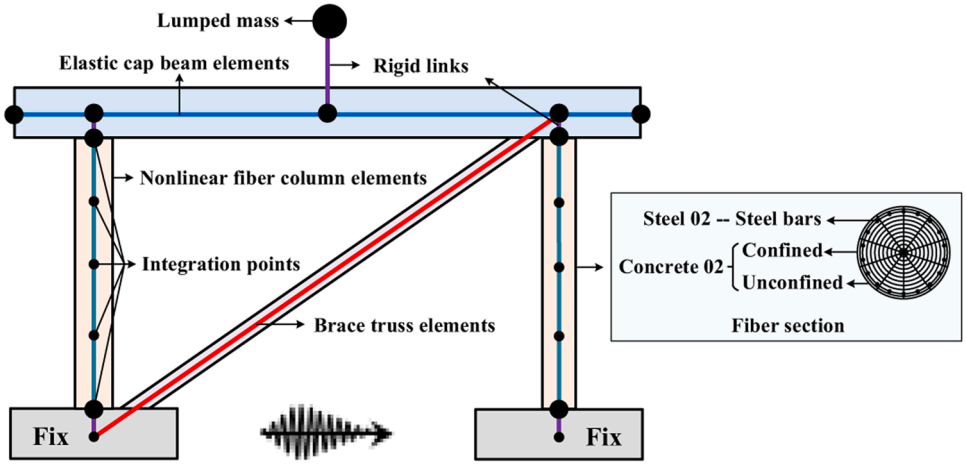

Fig. 13. The developed FE model of the bridge pier with brace in OpenSEES.

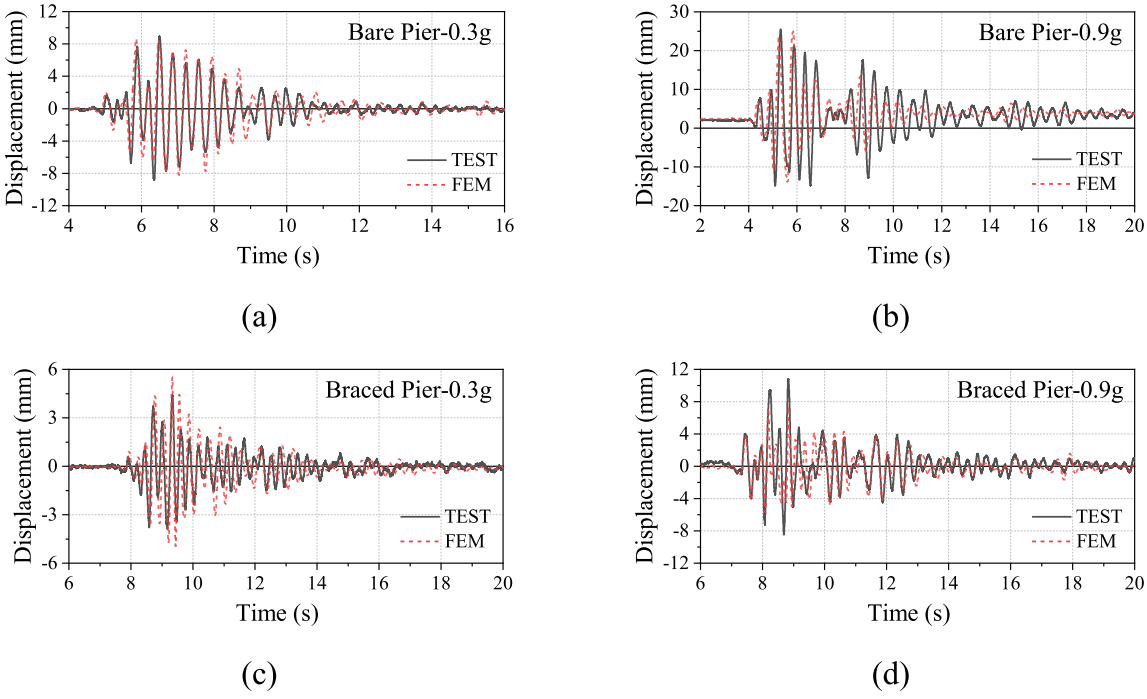

Fig. 15. Displacement response comparisons of the bare (a-b) and braced pier (c-d) under 0.3 g and 0.9 g excitations.

Table 4
Key parameters of the brace.

Braces	Yield displacement δ_0 (mm)	Yield force F_y (kN)	Initial stiffness K_1 (kN/mm)	Post yield stiffness K_2 (kN/mm)	Post yield stiffness ratio	Energy dissipation ratio β
Specimen	0.55	47.00	85.50	1.54	0.018	0.25
Prototype	17.54	1500.00	85.50	1.54	0.018	0.25

parameters of the scaled brace are also provided in Table 4.

5.2. Selection of input ground motions

Current seismic design specifications are generally based on far-field ground motions. Actually, the near-fault pulse-like ground motions are normally more devastating for civil engineering structures [49] due to the existence of velocity pulses in this type of motions [50,51]. Therefore, a total of 20 near-fault pulse-like ground motions, characterized by substantial velocity pulses, are selected from the PEER (Pacific Earthquake Engineering Research Centre) database in the present study. These ground motions are recorded within a distance of 30 km [52] from the rupture fault, with earthquake magnitudes (Mw) ranging from 5.74 to 7.62. The original peak ground accelerations (PGA) of these records vary between 0.15 g to 1.22 g. Table 5 summarizes the basic information for the selected ground motions. Fig. 16 presents the 5.0 %

Table 5
Characteristics of the selected 20 near-fault ground motions.

No.	RSN	Event	Year	Station	Tp	Magnitude	Mechanism	Rrup (km)	PGA(g)	PGV/PGA
NF1	77	San Fernando	1971	Pacoima Dam (upper left abut)	1.64	6.61	Reverse	1.81	1.22	0.10
NF2	143	Tabas_ Iran	1978	Tabas	6.19	7.35	Reverse	2.05	0.85	0.12
NF3	149	Coyote Lake	1979	Gilroy Array #4	1.35	5.74	strike slip	5.70	0.23	0.11
NF4	182	Imperial Valley−06	1979	El Centro Array #7	4.38	6.53	strike slip	0.56	0.34	0.15
NF5	459	Morgan Hill	1984	Gilroy Array #6	1.23	6.19	strike slip	9.87	0.22	0.05
NF6	569	San Salvador	1986	National Geografical Inst	1.13	5.8	strike slip	6.99	0.40	0.14
NF7	723	Superstition Hills−02	1987	Parachute Test Site	2.39	6.54	strike slip	0.95	0.43	0.32
NF8	803	Loma Prieta	1989	Saratoga - W Valley Coll.	5.65	6.93	Reverse Oblique	9.31	0.26	0.17
NF9	900	Landers	1992	Yermo Fire Station	7.50	7.28	strike slip	23.62	0.24	0.21
NF10	1013	Northridge−01	1994	LA Dam	1.62	6.69	Reverse	5.92	0.43	0.18
NF11	1045	Northridge−01	1994	Newhall - W Pico Canyon Rd.	2.98	6.69	Reverse	5.48	0.42	0.29
NF12	1084	Northridge−01	1994	Sylmar - Converter Sta	2.98	6.69	Reverse	5.35	0.62	0.19
NF13	3965	Tottori_ Japan	2000	TTR008	1.54	6.61	strike slip	6.88	0.32	0.11
NF14	4040	Bam_ Iran	2003	Bam	2.02	6.6	strike slip	1.70	0.81	0.16
NF15	4113	Parkfield−02_ CA	2004	Parkfield - Fault Zone 9	1.13	6.0	strike slip	2.85	0.15	0.16
NF16	4228	Niigata_Japan	2004	NIGH11	1.80	6.63	Reverse	8.93	0.46	0.08
NF17	4458	Montenegro_ Yugoslavia	1979	Ulcinj - Hotel Olimpic	1.97	7.1	Reverse	5.76	0.29	0.15
NF18	4847	Chuetsu-oki_ Japan	2007	Joetsu Kakizakiku Kakizaki	1.40	6.8	Reverse	11.94	0.30	0.16
NF19	6927	Darfield_ New Zealand	2010	LINC	7.37	7.0	strike slip	7.11	0.46	0.24
NF20	8119	Christchurch_ New Zealand	2011	Pages Road Pumping Station	4.82	6.2	Reverse Oblique	1.98	0.60	0.14

damped elastic response spectrums of these selected ground motions along with their mean spectrum. It should be noted that fault mechanism, the main source of dispersion in the response spectra of different ground motions, is not set as a condition when earthquake ground motions are selected, due to the fact that the main purpose of the present study is to investigate the effectiveness of the developed novel CP-SCED brace.

Due to the bridge piers are constructed in southwest China, a location characterized by high seismic hazard level, the input PGA level of all motions is scaled to 0.6 g in the following analysis, corresponding to severe earthquakes with return period of 2475 years specified in Chinese code [53] for this region [54].

5.3. Influences of design parameters on the seismic performances of bridge piers

To better understand the influences of the brace design parameters on the seismic performance of bridge piers, extensive parametric analyses are conducted in this section. Three main parameters are utilized to characterize the CP-SCED brace, namely the ratio of the yield strength ratio α, the number of pulleys n and the energy dissipation ratio β. The definition, ranges of these parameters, as well as the corresponding symbols, are listed and explained in Table 6.

The CP-SCED brace offers significant benefits in reducing the peak displacement response of the pier by increasing the structural stiffness and dissipating a portion of the earthquake energy. Moreover, it effectively mitigates the residual deformation of the bridge pier due to its self-centering capability. However, the increased structural stiffness may substantially elevate the base shear force on the pier column, leading to potential damage in the plastic hinge areas. Consequently, in the seismic performance evaluation of braced piers, it is imperative to consider both peak and residual drift ratios, along with the peak base shear force in the columns. Three evaluation indices have been defined for this purpose, encompassing the peak and residual drift ratios at the pier top and the ratio of peak base shear force between bare and braced columns. Through analyses, a comprehensive understanding on how the brace influences the seismic response of the bridge pier can be achieved. These analyses allow for the proper selection of optimal design parameters, ensuring the brace to exhibit optimal control performance.

Figs. 17–19 present the evaluation indices versus n and β for a variety of α values when the structure is subjected to the near-fault ground motions as listed in Table 4. The three evaluation indices include the averaged peak drift ratio, residual drift ratio and ratio of the peak shear force over the 20 ground motions for each case. Furthermore,

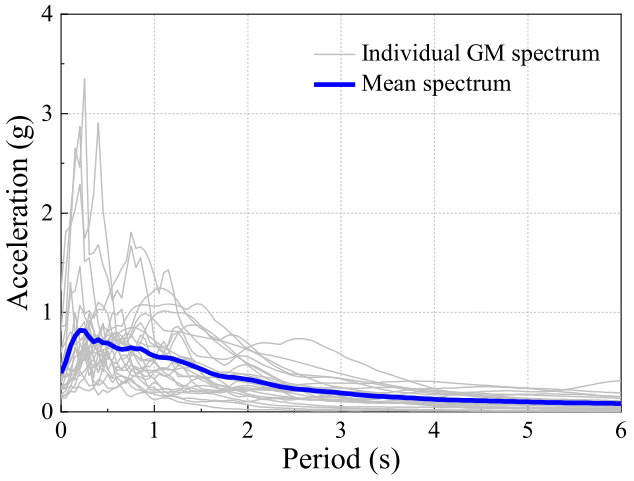

Fig. 16. Acceleration response spectra for the selected 20 ground motions and the mean spectrum.

Table 6
Parameters of CP-SCED brace considered for analysis.

Symbol	Definition	Notation
α	Ratio of the yield strength of brace to that of bare pier	0.5,1.0 and 1.5
n	The number of the pulleys	0–10 with interval of 1
β	Energy dissipation capacity of the brace	0.0–2.0 with interval of 0.1

for comparison, the results for the bare pier are also presented, and they are shown by the gray flat planes in the 3D surface plots.

Fig. 17 shows the peak drift ratios as a function of α, n and β. As shown, the demand for peak drift ratios of braced piers with different α exhibit a similar trend, and it is significantly influenced by both parameters n and β. Higher values of n, β, and α lead to a notable reduction in the peak displacement of the structure. This reduction can be attributed to the increased stiffness of the structure with higher n. Additionally, increased β values enhance the energy dissipation capacity of the brace, resulting in less seismic energy being transferred to the piers. Regarding the parameter α, this decrease can be explained by that the brace enhances the system resistance to yielding. However, it is essential to note that increasing the yield strength of the brace comes at the expense of the peak force increment and ultimate deformation decrement of the brace. For the bare pier, as shown in Fig. 17, the peak drift ratio reaches 4.4 %, which can be regarded as collapsed according to Uma et al. [55] (who concluded that when the peak lateral displacement ratio of the structure exceeds 4.0 %, it has collapsed). In contrast, the peak drift ratios for all the considered braced piers are less than 4.0 %, indicating the collapse potential of the pier has been significantly reduced. In other words, through the rational design of brace parameters, the peak displacement response of the structure can be effectively controlled.

Fig. 18 illustrates the impacts of n, β, and α on the structural residual displacement. It can be seen that larger values of n and α, coupled with smaller β, can effectively minimize the residual deformation. This is because a larger n results in a greater post-yield stiffness, which in turn reduces the peak displacement response as discussed above, thus decreases the extent of plastic damage of the structure and suppresses the generation of residual deformation. Moreover, larger α and smaller β provide greater self-restoring force, aiding in pulling the pier back to its original position and eliminating the residual deformation.

The results also suggest that under (dynamic) seismic excitation, when the brace self-restoring force (F_r) is less than the yield force of the bridge pier, the residual deformation of the bridge pier can still be effectively controlled. For example, under conditions of $\alpha = 1.0$ and $n = 1.0$, when $\beta = 1.0$, the F_r value is 0.0 kN (refer to Fig. 1), indicating that the brace cannot help the pier reduce the residual deformation, the residual drift ratio of the pier is 0.05 % only as shown in Fig. 18(b). From $\beta = 1.6$, as β increases further, there is a noticeable increase in residual deformation. When $\beta = 1.8$, F_r is −163.92 kN, signifying that the self-centering system of the brace cannot pull the brace back to its original position and even potentially exacerbating the residual deformation of the piers. However, at this point, the residual drift ratio of the braced pier is only 0.18 % as shown in Fig. 18(b) again. According to studies by Uma et al. [55] and Kam et al. [56], if only considering residual deformation as the damage indicator, the structure functions well (less than or equal to 0.2 %), requiring no repair or reinforcement to meet normal usage requirements. When $\beta = 1.9$, the residual drift ratio reaches 0.22 %, implying that the structure needs minor repair or reinforcement at this time. The reason is that, unlike static analysis, the residual deformation of the structure is closely related to the input ground motion characteristics. Moreover, as mentioned previously, the structure exhibits 'probabilistic self-centering' in dynamic loading, indicating a tendency to return to its original position after significant displacement. Although the F_r may not fully restore the structure under

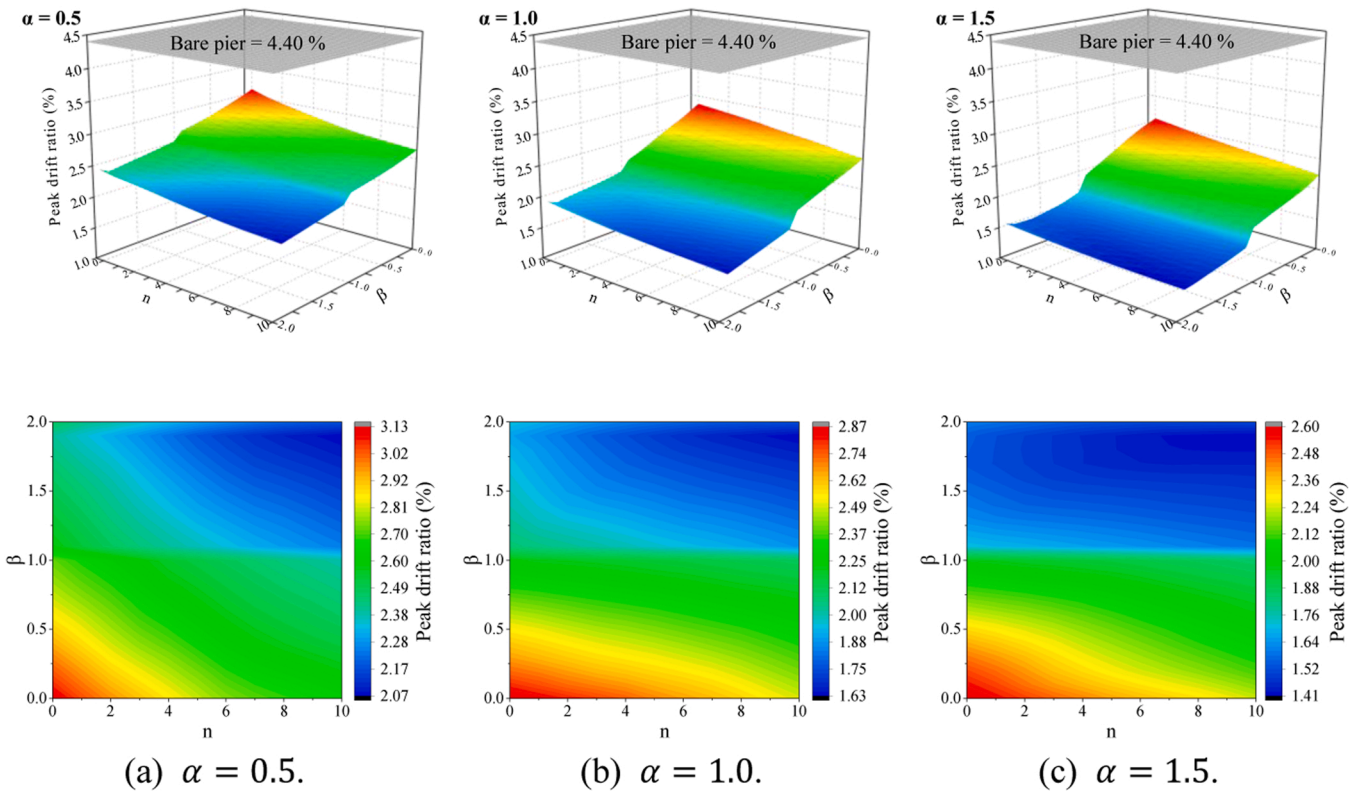

Fig. 17. Peak drift ratios versus α, n and β. Top: 3D plot & Bottom: Contour plot.

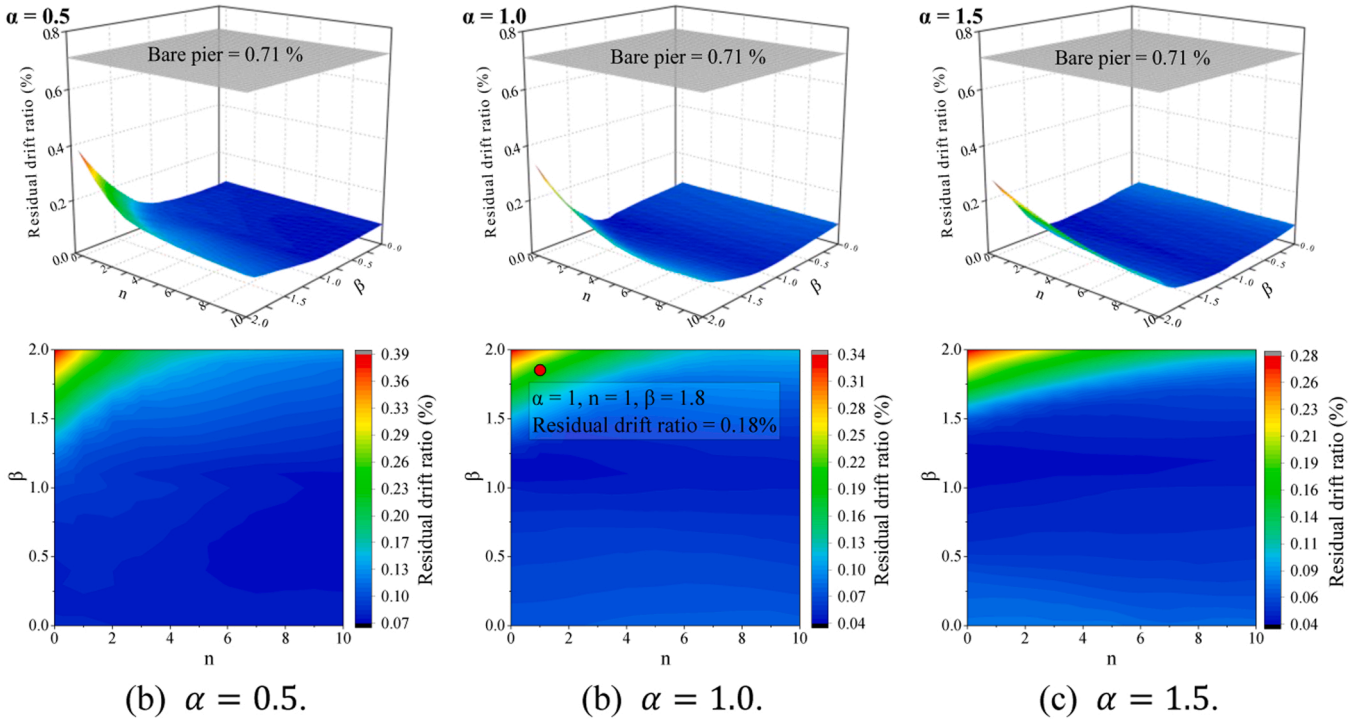

Fig. 18. Residual drift ratios versus α, n and β. Top: 3D plot & Bottom: Contour plot.

static loading, it is still possible for the residual displacement to be 'zero' under seismic loading. Therefore, in the design process, while meeting the requirement for residual deformation, it is advisable to appropriately increase β to enhance the brace energy dissipation capacity, thereby reducing the structural peak displacement response.

Fig. 19 illustrates the influence of brace design parameters on the base shear force in pier. It is evident that an increase in n and α leads to a significant increase in base shear force demand. This is because increasing n enlarges the brace post-yield stiffness, thereby enhancing the overall stiffness of the braced pier. Similarly, increasing α increases

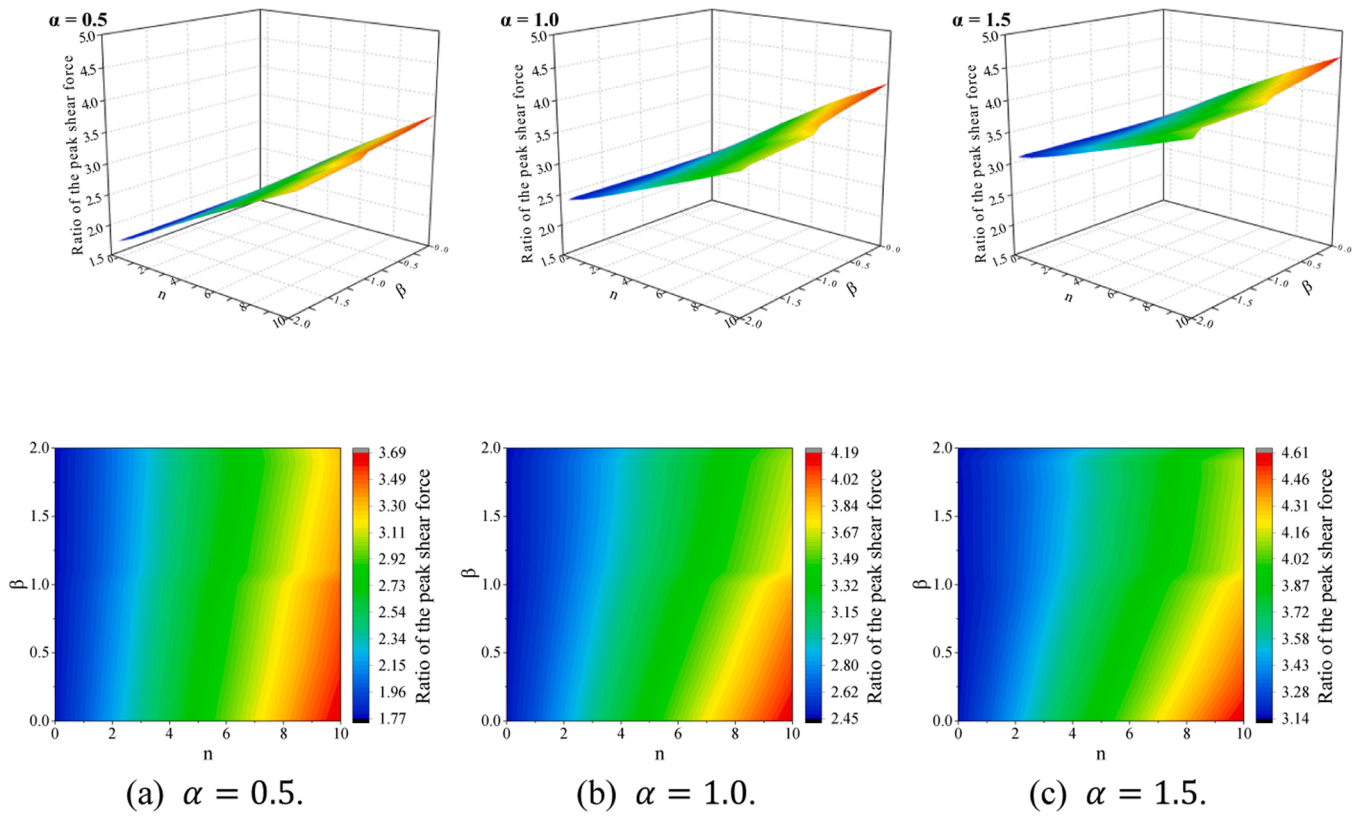

Fig. 19. Ratio of the peak shear force versus α, n and β. Top: 3D plot & Bottom: Contour plot.

the brace yield strength, consequently leading to an increase in the load-bearing capacity of the braced pier. Conversely, for β, it has minimal effect on the base shear force, with only a slight decrease as β increases. This reduction may be attributed to the fact that the brace with a larger β dissipates more energy, thus reduces the peak displacement response of the bridge pier. As the brace post-yield stiffness is greater than 0.0, the smaller peak displacement results in lower shear force. In short, the installation of braces will affect the shear distribution, elevating the risk of plastic hinge area damage, thus necessitating careful consideration during the design phase.

In summary, the preceding analysis highlights the varying impacts of different design parameters on various damage indicators. A comprehensive consideration of these factors is crucial to strike a balance between the seismic performance in displacement responses and column

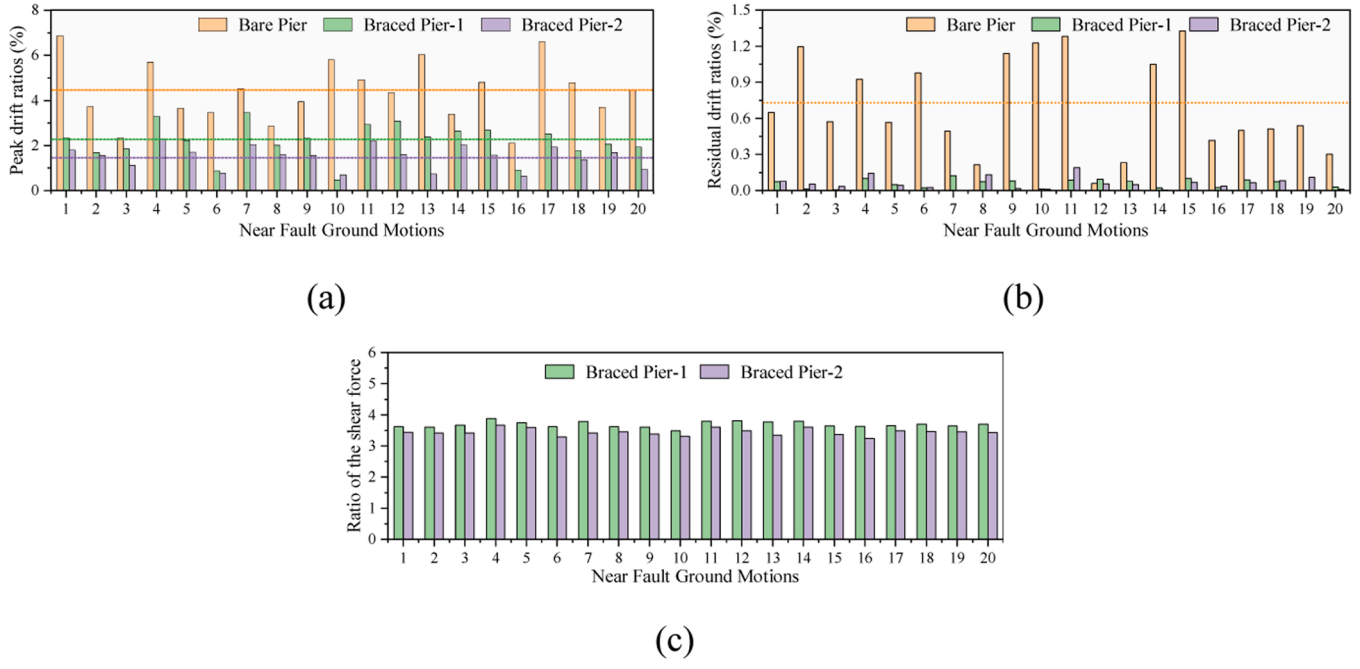

Fig. 20. Comparison of three types bridge piers response under 20 ground motions:(a) peak drift ratios, (b) residual drift ratios and (c) peak base shear force.

damage. During the design process, the following guide principle is suggested: while meeting peak displacement and residual deformation requirements, minimize the brace influence on base shear force as much as possible. This can be achieved through the following steps: (1) Ensuring compliance with residual drift ratio requirement; (2) Meeting peak drift ratio requirement; (3) Finally, selecting the minimum peak base shear force. A thorough assessment of the calculated results suggests that, for the example pier discussed in this article, the ideal design values can be taken as $n = 3$, $\beta = 1.6$, and $\alpha = 1.5$.

5.4. Design efficiency verification

This section verifies the design parameters provided in the previous section through comparing the responses of the bare pier and two types of braced piers. Fig. 20 presents the maximum values of damage indices (peak and residual drift ratios, peak base shear force) under the 20 near-fault ground motions. Specifically, 'Bare Pier' represents the outcomes of the bridge pier without brace, while 'Braced Pier-1' and 'Braced Pier-2' depict the bridge pier with brace design parameters determined by the 'fully self-centering' approach and 'recommended values' obtained in the previous section, respectively. To facilitate comparison, the two types of the design parameters are summarized in Table 7.

From Fig. 20 (a) and (b), it is evident that the bare pier exhibits the largest peak and residual drift ratios among these three types of bridge piers. This suggests that the braces effectively reduce both the peak and residual displacement responses for each considered ground motion. The average peak drift ratios are 4.40 % (Bare Pier), 2.17 % (Braced Pier-1), and 1.49 % (Braced Pier-2), with corresponding average residual drift ratios of 0.71 %, 0.06 %, and 0.06 %, respectively. However, the braces also lead to a significant increase in base shear force demand. As observed in Fig. 20(c), the average base shear force is amplified by 3.69 times (Braced Pier-1) and 3.44 times (Braced Pier-2), respectively.

In summary, the following conclusions can be drawn: (1) The peak drift ratio of the Braced Pier-2 is smaller than that of Braced Pier-1, with the former being 68.66 % of the latter. This is due to Brace-2 having a higher β as compared to Brace-1, resulting in greater energy dissipation by the brace. Additionally, Brace-2 has a larger post-yield stiffness, thereby increasing the overall stiffness of the bridge pier. (2) Despite Brace-2 having a negative F_r ($\beta = 1.6$), its mean residual deformation is the same as that of Braced Pier-1. This confirms the previous conclusion that a partially self-centering design can reduce peak displacement response without increasing residual deformation. (3) Although the Brace-2 has a larger k_{s2}, due to the lower yield strength of the brace-2 and the smaller peak displacement response of Braced Pier-2, the base shear demand is smaller compared to Braced Pier-1. However, it should be noted that regardless of the brace parameters used, the base shear of the pier will be amplified, which is unavoidable. In design, attention should be paid to directly connecting the brace to the foundation and cap beam of the pier to reduce damage to the plastic hinge area of the columns. Overall, a design that considers the coupling influences of the three parameters is more effective in utilizing the brace hysteresis performance and enhancing the seismic performance of the bridge pier.

6. Conclusions

Energy dissipation braces are widely used to control the seismic induced damages of engineering structures. Different brace parameters could affect different damage indices in distinct ways. It is essential to comprehensively consider these parameters to optimally control the structural responses and ensure the best seismic performance. This study proposes a parameter-adjustable CP-SCED brace capable of modifying its hysteretic parameters as needed. The working mechanism and analytical model of the brace are introduced. The influences of the key design parameters of the brace on the seismic responses of a double-column bridge pier are investigated in detail. The following conclusions can be drawn based on the analyses:

1. The design of the proposed CP-SCED brace is straightforward, with a clear working mechanism. Its yield strength, post-yield stiffness, and energy dissipation ratio can be easily adjusted. This offers designers increased flexibility, enabling comprehensive consideration of various damage indicators to ensure structural damage remains within acceptable limits. Moreover, this adaptability enables the brace to be applied to a broader range of structures;

2. The proposed analytical model can accurately predict the hysteretic behavior of the CP-SCED brace. Parametric analyses indicate that by adjusting various features of the brace, including the initial pre-compressive force of the two disc-spring groups, the number of pulleys fixed on the middle shim plate, and the force required to activate the two external friction devices, different hysteretic performance can be achieved;

3. The brace with a larger α makes the system more resistant to yielding, reducing both peak and residual drift ratios, but increases the base shear force of the bridge piers. A larger n enhances the brace post-yield stiffness, increases the overall stiffness of the structure, thus reduces the peak and residual deformations. However, this design results in a higher base shear force. A larger β indicates a greater energy dissipation capacity of the brace, significantly reducing the peak displacement and base shear force of the structure. Nonetheless, when β exceeds a certain value (1.6), the residual deformation of the structure increases significantly.

4. Through comprehensive system-level analyses, optimal parameter values ($n = 3$, β=1.6, and α=1.5) are suggested. The 'partial self-centering' brace effectively minimizes peak displacement response in piers without increasing the residual deformation. The average peak drift ratio of Braced Pier-2 is 68.66 % of Braced Pier-1, while the average residual drift ratio remains constant at 0.06 %. Additionally, although Brace-2 has a larger post-yield stiffness, it also reduces the demand for the brace yield strength. As a result, the average peak base shear force is reduced by 6.78 % compared to Braced Pier-1. These results highlight the roles of the cable-pulley system. In a short, the hysteresis performance of the brace is fully utilized, achieving favorable damage control effects.

In summary, this study enhances our understanding on how the design parameters of CP-SCED brace impact the seismic responses of bridge piers. It provides valuable guidance for applying this novel brace in seismic-resistant bridge pier designs. It is important to note that this research examines design parameters deterministically, without fully considering the uncertainties in structural geometry and the randomness of earthquake excitations. Future studies will explore probabilistic approaches (e.g., fragility analysis methods), providing more comprehensive insights into these issues.

This study primarily focuses on the configuration, working mechanism, and analytical model of the CP-SCED brace. It is important to emphasize that, in engineering practices, issues such as bearing failures, connection detachment, and cable misalignment may occur under certain conditions. These issues should be further investigated in the

Table 7
Key parameters of the two braces.

Braces	Yield displacement μ_{sy} (mm)	Yield force f_{sy} (kN)	Initial stiffness k_{s1} (kN/mm)	Post yield stiffness k_{s2} (kN/mm)	Post yield stiffness ratio	Energy dissipation ratio β
Brace−1	17.54	1500.00	85.50	1.54	0.018	0.25
Brace−2	14.38	1229.42	85.50	3.08	0.036	1.60

future studies.

Declaration of Competing Interest

The authors declare that they have no known competing financial interests or personal relationships that could have appeared to influence the work reported in the paper.

Acknowledgments

The authors would like to acknowledge the support from National Natural Science Foundation of China (Nos. 51778023, 52078019 and 52278475) for carrying out this research. The authors also acknowledge the financial support of the China Scholarship Council (CSC) for Huailei Qin to visit Politecnico di Milano, Italy (Grant No. 202206540043).

Data availability

Data will be made available on request.

References

[1] McCormick J, Aburano H, Ikenaga M, Nakashima M. Permissible residual deformation levels for building structures considering both safety and human elements. Proc. 14th World Conf. Earthquake Engineering. Beijing: Seismological Press of China; 2008. Paper ID 05-06-0071.
[2] Maffei J, Telleen K, Nakayama Y. Probability-based seismic assessment of buildings, considering post-earthquake safety. Earthq Spectra 2008;24(3):667–99. https://doi.org/10.1193/1.2950066.
[3] Yousef-beik SMM, Veismoradi S, Zarnani P, Quenneville P. A new self-centering brace with zero secondary stiffness using elastic buckling. J Constr Steel Res 2020; 169:106035. https://doi.org/10.1016/j.jcsr.2020.106035.
[4] Xu LH, Fan XW, Li ZX. Seismic assessment of buildings with prepressed spring self-centering energy dissipation braces. J Struct Eng 2020;146(2):04019190. https://doi.org/10.1061/(ASCE)ST.1943-541X.0002493.
[5] Xu LH, Fan XW, Li ZX. Development and experimental verification of a pre-pressed spring self-centering energy dissipation brace. Eng Struct 2016;127:49–61. https://doi.org/10.1016/j.engstruct.2016.08.043.
[6] Dong H, Du X, Han Q, Hao H, Bi K, Wang X. Performance of an innovative self-centering buckling restrained brace for mitigating seismic responses of bridge structures with double-column piers. Eng Struct 2017;148:47–62. https://doi.org/10.1016/j.engstruct.2017.06.011.
[7] Miller DJ, Fahnestock LA, Eatherton MR. Development and experimental validation of a nickel–titanium shape memory alloy self-centering buckling-restrained brace. Eng Struct 2012;40:288–98. https://doi.org/10.1016/j.engstruct.2012.02.037.
[8] Wang W, Fang C, Zhang A, Liu X. Manufacturing and performance of a novel self-centring damper with shape memory alloy ring springs for seismic resilience. Struct Control Health Monit 2019;26(5):e2337. https://doi.org/10.1002/stc.2337.
[9] Rahgozar N, Shahria Alam M. A novel hybrid self-centering piston-based bracing fitted with SMA bars and friction springs: analytical study and seismic simulation. J Struct Eng 2023;149(6):04023055. https://doi.org/10.1061/JSENDH.STENG-11938.
[10] Xie Q, Zhou Z, Meng S-P. Experimental investigation of the hysteretic performance of self-centering buckling-restrained braces with friction fuses. Eng Struct 2020; 203:109865. https://doi.org/10.1016/j.engstruct.2019.109865.
[11] Zhou Z, Xie Q, Lei XC, He XT, Meng SP. Experimental investigation of the hysteretic performance of dual-tube self-centering buckling-restrained braces with composite tendons. J Compos Constr 2015;19(6):04015011. https://doi.org/10.1061/(ASCE)CC.1943-5614.0000565.
[12] Huang H, Zhang F, Zhang W, Guo M, Urushadze S, Wu G. Numerical analysis of self-centering energy dissipation brace with arc steel plate for seismic resistance. Soil Dyn Earthq Eng 2019;125:105751. https://doi.org/10.1016/j.soildyn.2019.105751.
[13] Zhang C, Zong S, Sui Z, Guo X. Seismic performance of steel braced frames with innovative assembled self-centering buckling restrained braces with variable post-yield stiffness. J Build Eng 2023;64:105667. https://doi.org/10.1016/j.jobe.2022.105667.
[14] Qiu CX, Yang Y, Liu J, Jiang T. Test of a novel self-centering brace using SMA slip friction damper. J Constr Steel Res 2023;204:107872. https://doi.org/10.1016/j.jcsr.2023.107872.
[15] Xue D, Bi K, Dong H, Qin H, Han Q, Du X. Development of a novel self-centering slip friction brace for enhancing the cyclic behaviors of RC double-column bridge bents. Eng Struct 2021;232:111838. https://doi.org/10.1016/j.engstruct.2020.111838.
[16] Lu X, Lv Z, Lv Q. Self-centering viscoelastic diagonal brace for the outrigger of supertall buildings: development and experiment investigation. Struct Des Tall Spec Build 2020;29(1). https://doi.org/10.1002/tal.1684.
[17] Silwal B, Michael RJ, Ozbulut OE. A superelastic viscous damper for enhanced seismic performance of steel moment frames. Eng Struct 2015;105:152–64. https://doi.org/10.1016/j.engstruct.2015.10.005.
[18] Yan X, Shu G, Rahgozar N, Alam MS. Seismic design and performance evaluation of hybrid braced frames having buckling-restrained braces and self-centering viscous energy-dissipative braces. J Constr Steel Res 2024;213:108359. https://doi.org/10.1016/j.jcsr.2023.108359.
[19] Yan X, Rahgozar N, Alam MS. Seismic life-cycle cost evaluation of steel-braced frames: comparing conventional BRBF with emerging SCVDF and HBF systems. Eng Struct 2024;313:118256. https://doi.org/10.1016/j.engstruct.2024.118256.
[20] Dong H, Du X, Han Q, Bi K. Numerical studies on the seismic performances of RC two-column bent bridges with self-centering energy dissipation braces. J Struct Eng 2020;146(4):04020038. https://doi.org/10.1061/(ASCE)ST.1943-541X.0002587.
[21] Wang W, Fang C, Shen D, Zhang R, Ding J, Wu H. Performance assessment of disc spring-based self-centering braces for seismic hazard mitigation. Eng Struct 2021; 242:112527. https://doi.org/10.1016/j.engstruct.2021.112527.
[22] Kari A, Ghassemieh M, Abolmaali SA. A new dual bracing system for improving the seismic behavior of steel structures. Smart Mater Struct 2011;20(12):125020. https://doi.org/10.1088/0964-1726/20/12/125020.
[23] Qiu CX, Zhu S. High-mode effects on seismic performance of multi-story self-centering braced steel frames. J Constr Steel Res 2016;119:133–43. https://doi.org/10.1016/j.jcsr.2015.12.008.
[24] Dong H, Wen J, Han Q, Du X. Seismic performance assessment of a rc bridge retrofitted with SCEBs under near-fault pulse-like ground motions. J Earthq Eng 2023;27(13):3705–27. https://doi.org/10.1080/13632469.2022.2144964.
[25] Erochko J, Christopoulos C, Tremblay R, Kim HJ. Shake table testing and numerical simulation of a self-centering energy dissipative braced frame. Earthq Eng Struct Dyn 2013;42(11):1617–35. https://doi.org/10.1002/eqe.2290.
[26] Araki Y, Shrestha KC, Maekawa N, Koetaka Y, Omori T, Kainuma R. Shaking table tests of steel frame with superelastic Cu–Al–Mn SMA tension braces. Earthq Eng Struct Dyn 2016;45(2):297–314. https://doi.org/10.1002/eqe.2659.
[27] Qiu C, Zhu S. Shake table test and numerical study of self-centering steel frame with SMA braces: self-centering steel frame with SMA braces. Earthq Eng Struct Dyn 2017;46(1):117–37. https://doi.org/10.1002/eqe.2777.
[28] Rafi MM, Lodi SH, Al-Sadoon ZA, Saatcioglu M, Palermo D. Experimental investigation of dynamic behavior of RC frame strengthened with buckling-restrained bracing. J Struct Eng 2022;148(7):04022076. https://doi.org/10.1061/(ASCE)ST.1943-541X.0003371.
[29] Issa A, Rahgozar N, Alam MS. Experimental investigation and seismic analysis of a novel self-centering piston-based bracing archetype with polyurethane cores. Eng Struct 2023;283:115735. https://doi.org/10.1016/j.engstruct.2023.115735.
[30] Upadhyay A., Asce S.M., Pantelides C.P., Student G."Comparison of the seismic retrofit of a three-column bridge bent with buckling restrained braces and self centering braces." Structures congress 2017 Denver, Colorado: American Society of Civil Engineers; 2017. pp. 414–423. https://doi.org/10.1061/9780784480403.035..
[31] Upadhyay A, Pantelides CP, Ibarra L. Residual drift mitigation for bridges retrofitted with buckling restrained braces or self-centering energy dissipation devices. Eng Struct 2019;199:109663. https://doi.org/10.1016/j.engstruct.2019.109663.
[32] Xiang N, Alam MS. Displacement-based seismic design of bridge bents retrofitted with various bracing devices and their seismic fragility assessment under near-fault and far-field ground motions. Soil Dyn Earthq Eng 2019;119:75–90. https://doi.org/10.1016/j.soildyn.2018.12.023.
[33] Dong H, Du X, Han Q, Bi K, Hao H. Hysteretic performance of RC double-column bridge piers with self-centering buckling restrained braces. Bull Earthq Eng 2019; 17(6):3255–81. https://doi.org/10.1007/s10518-019-00586-4.
[34] Bi K, Li C, Hao H. State-of-the-art review of the seismic performance of precast segmental columns. Adv Bridg Eng 2022;3.
[35] Dong H, Wang C, Han Q, Du X. Re-centering capability of partially self-centering structures with flag-shaped hysteretic behavior subjected to near-fault pulsed ground motion. Soil Dyn Earthq Eng 2024;186:108892. https://doi.org/10.1016/j.soildyn.2024.108892.
[36] Khaneghah MA, Dehcheshmaeh EM, Broujerdian V, Amiri GG. Optimized design of dual steel moment resisting system equipped with cross-anchored self-centering buckling restrained chevron brace. Earthq Struct 2022;23(2):139. https://doi.org/10.12989/eas.2022.23.2.139.
[37] Jalilzadeh M, Ahadpour Khaneghah M, Safari P, Broujerdian V, Ghamari A. Investigating the seismic performance of disc spring-based self-centering bracing system. Int J Civ Eng 2024:1–21. https://doi.org/10.1007/s40999-024-01022-8.
[38] Xu LH, Fan XW, Li ZX. Cyclic behavior and failure mechanism of self-centering energy dissipation braces with pre-pressed combination disc springs. Earthq Eng Struct Dyn 2016;46:1065–80. https://doi.org/10.1002/eqe.2844.
[39] Hernandez F, Astroza R, Beltran JF, Zhang X, Mercado V. A experimental study of a cable-pulleys spring-damper energy dissipation system for buildings. J Build Eng 2022;51:104034.
[40] Jung IY, Ryu J, Oh J, Ryu D, Ko H. Experimental investigation on displacement amplification mechanism of steel wire rope-pulley damping systems with viscous damper. Eng Struct 2021;248113206.
[41] Majima R, Hayashi K, Saito T. Development of new passive vibration control system in coupled structures with block and tackle. Soil Dynam Earthq Eng 2022; 159:107319.
[42] Majima R, Haruyama T, Sakai S, Yamasaki Y, Saito T. Shake table tests on a new passively controlled system with pulley amplification mechanisms for suspended ceilings. World Conf Seism Isol 2022:696–706.

[43] Eatherton M.R., Hajjar J.F."Residual drifts of self-centering systems including effects of ambient building resistance." Earthquake Spectra, 27 (3): pp. 719–744. SAGE Publications Sage UK: London, England. https://doi.org/10.1193/1.36053182011.
[44] Fang C, Zhong Q, Wang W, Hu S, Qiu C. Peak and residual responses of steel moment-resisting and braced frames under pulse-like near-fault earthquakes. Eng Struct 2018;177:579–97. https://doi.org/10.1016/j.engstruct.2018.10.013.
[45] Atasever K, Inanaga S, Takeuchi T, Terazawa Y, Celik OC. Experimental and numerical studies on buckling restrained braces with posttensioned carbon fiber composite cables. Earthq Engng Struct Dyn 2020;49(15):1640–61. https://doi.org/10.1002/eqe.3321.
[46] Qin H, Bi K, Dong H, Han Q, X, Du X. "Shake table tests on RC double-column bridge piers with self-centering energy dissipation braces.". J Bridge Eng 2023;28(8):04023049. https://doi.org/10.1061/JBENF2.BEENG-6069.
[47] Standard Chinese. Disc springs. GB/T 1972-2005. Beijing: Chinese Standard.; 2005.
[48] Erochko J, Christopoulos C, Tremblay R. Design, testing, and detailed component modeling of a high-capacity self-centering energy-dissipative brace. J Struct Eng 2015;141(8):04014193. https://doi.org/10.1061/(ASCE)ST.1943-541X.0001166.
[49] Chen X, Li C. Seismic assessment of earthquake-resilient tall pier bridges using rocking foundation retrofitted with various energy dissipation devices. Struct Control Health Monit 2020;27(11). https://doi.org/10.1002/stc.2625.
[50] Bray JD, Rodriguez-Marek A. Characterization of forward-directivity ground motions in the near-fault region. Soil Dyn Earthq Eng 2004;24(11):815–28. https://doi.org/10.1016/j.soildyn.2004.05.001.
[51] Phan V, Saiidi MS, Anderson J, Ghasemi H. Near-fault ground motion effects on reinforced concrete bridge columns. J Struct Eng 2007;133(7):982–9. https://doi.org/10.1061/(ASCE)0733-9445(2007)133:7(982).
[52] Dabaghi M, Der Kiureghian A. Stochastic model for simulation of near-fault ground motions: stochastic model for simulation of near-fault ground motions. Earthq Eng Struct Dyn 2017;46(6):963–84. https://doi.org/10.1002/eqe.2839.
[53] People's Republic of China Ministry of Transport. Guidelines for seismic design of highway bridges JTG/T B02–01-2008. Beijing: China Communications Press; 2008.
[54] Chen X, Domenico D, Li C. Seismic resilient design of rocking tall piers using inerter-based systems. Eng Struct 2023;281:115819. https://doi.org/10.1016/j.engstruct.2023.115819.
[55] Uma S, Pampanin S, Christopoulos C. Development of probabilistic framework for performance-based seismic assessment of structures considering residual deformations. J Earthq Eng 2010;14(7):1092–111. https://doi.org/10.1080/13632460903556509.
[56] Kam W.Y., Pampanin S., Palermo A., Carr A. Design procedure and behaviour of advanced flag-shape (AFS) MDOF systems. New Zealand Society of Earthquake Engineering (NZSEE) Conference, Wairakei, New Zealand. 2008.